

AD A 038917

12

FL

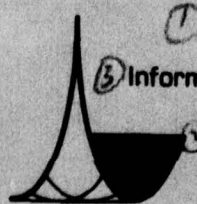


DIV 2

DDC
RECEIVED
MAY 3 1977
A

AD No. _____
DDC FILE COPY,

410 168 New



① **ENSCO, INC.**

③ Information & System Sciences Division

8001 Forbes Place
Springfield, Virginia 22151

Phone: (703) 569-9000

DISTRIBUTION STATEMENT A
Approved for public release;
Distribution Unlimited

12

IMPROVED PROCEDURES FOR
DETERMINING SEISMIC SOURCE DEPTHS FROM
DEPTH PHASE INFORMATION

FINAL REPORT

Edward A. Page

101473

July 1976

DDC
RECEIVED
MAY 3 1977
A

Sponsored by:

Advanced Research Project Agency
ARPA Order No. 2251

APPROVED FOR PUBLIC
RELEASE. DISTRIBUTION UNLIMITED.

Handwritten signature

Notice of Disclaimer

The views and conclusions contained in this document are those of the author and should not be interpreted as necessarily representing the official policies, either expressed or implied, of the Advanced Research Project Agency, the Air Force Technical Applications Center, or the U.S. government.

WFO	White Section	<input checked="" type="checkbox"/>
DOB	Blue Section	<input type="checkbox"/>
UNKNOWN		<input type="checkbox"/>
JUSTIFICATION		
BY		
DISTRIBUTION/AVAILABILITY CODES		
Dist.	AVAIL. and/or SPECIAL	
<i>A</i>		

REPORT DOCUMENTATION PAGE		READ INSTRUCTIONS BEFORE COMPLETING FORM
1. REPORT NUMBER 6	2. GOVT ACCESSION NO.	3. RECIPIENT'S CATALOG NUMBER
4. TITLE (and Subtitle) Improved Procedures for Determining Seismic Source Depths from Depth Phase Information.		5. TYPE OF REPORT & PERIOD COVERED FINAL REPORT.
7. AUTHOR(s) Edward A. Page, Francis J. Cook, William J. Long		6. PERFORMING ORG. REPORT NUMBER N/A
9. PERFORMING ORGANIZATION NAME AND ADDRESS ENSCO, INC. <i>Information and System Sciences</i> 5408A Port Royal Road Springfield, Virginia 22151 <i>Div 410168</i>		8. CONTRACT OR GRANT NUMBER(s) F08606-76-C-0003, <i>Add</i>
11. CONTROLLING OFFICE NAME AND ADDRESS DCASD 300 E. Joppa Road, Room 200 Towson, Maryland 21204		10. PROGRAM ELEMENT, PROJECT, TASK AREA & WORK UNIT NUMBERS ✓ ARPA Order - 2551 VT/6710
14. MONITORING AGENCY NAME & ADDRESS (if different from Controlling Office) VELA Seismological Center 312 Montgomery Street Alexandria, Virginia 22314		12. REPORT DATE 30 June 1976
		13. NUMBER OF PAGES 67
		15. SECURITY CLASS. (of this report) (1268P.)
16. DISTRIBUTION STATEMENT (of this Report) APPROVED FOR PUBLIC RELEASE. DISTRIBUTION UNLIMITED.		15a. DECLASSIFICATION/DOWNGRADING SCHEDULE
17. DISTRIBUTION STATEMENT (of the abstract entered in Block 20, if different from Report)		
18. SUPPLEMENTARY NOTES		
19. KEY WORDS (Continue on reverse side if necessary and identify by block number) Seismic depth, depth phase, echo detection		
20. ABSTRACT (Continue on reverse side if necessary and identify by block number) The objective of this research is to develop an improved analysis procedure to determine teleseismic source depths from seismogram recordings. The analysis procedure is based on techniques developed by ENSCO, Inc. during two previous research efforts, and is to be automated. The purpose of this research is to substantially increase the percentage of events for which accurate source depths can be obtained, and to facilitate the analysis. (Continued)		

DD FORM 1 JAN 73 1473

EDITION OF 1 NOV 65 IS OBSOLETE

SECURITY CLASSIFICATION OF THIS PAGE (When Data Entered)

The primary concept involved in the improved techniques is the utilization of source depth information, contained throughout the seismic coda, which has previously either been ignored or improperly used. This information was utilized through the computation of travel times for the later arriving seismic phases and the development of techniques which improve the detection of these later phases.

The results of this research demonstrated that the automated source depth determination procedure constructively utilizes source depth information contained throughout the seismograms, and thereby significantly enhances source depth determinations. This was shown by obtaining the correct depth for an event through the separate analysis of the first and second minute of data, verifying the usefulness of source depth information contained in the later seismic phases. A further verification of the effectiveness of this procedure was achieved by obtaining correct depth estimates from data arriving through individual seismic phases, and from data recorded at individual stations.

During this contract, research was also coordinated which established possible modifications to these techniques which should enhance their effectiveness for events having shallow source depths.

SUBJECT: Improved Procedures for Determining Seismic
Source Depths from Depth Phase Information

AFTAC Project No.....	VELA T/6710
ARPA Order No.....	2551
ARPA Program Code No.....	6F10
Name of Contractor.....	ENSCO, INC.
Contract Number.....	F08606-76-C-0003
Effective Date of Contract.....	September 1, 1975
Report Period.....	September 1, 1975 to June 30, 1976
Amount of Contract.....	\$59,998
Contract Expiration Date.....	June 30, 1976
Project Scientist.....	Edward A. Page (703)321-9000

TABLE OF CONTENTS

	<u>Page</u>
1.0 INTRODUCTION	1-1
2.0 AUTOMATED SEISMIC SOURCE DEPTH ANALYSIS	2-1
2.1 Seismic Source Depth Analysis Procedures	2-1
2.2 Access and Storage of Differential Travel Time Information	2-5
3.0 APPLICATION OF THE ANALYSIS PROCEDURE TO THE ILLINOIS EVENT	3-1
4.0 SHALLOW SHOURCE DEPTH DETERMINATION USING CEPSTRUM ANALYSIS	4-1
4.1 Analysis of the Boxcar Event	4-1
4.2 Determination of the Effectiveness of Cepstrum Analysis for Shallow Source Depths Using Synthesized Data	4-10
5.0 CONCLUSION	5-1
APPENDIX A: COMPUTATION OF THE CEPSTRUM	A-1
APPENDIX B: COMPUTATION OF THE CEPSTRUM MATCHED FILTER	B-1

1.0 INTRODUCTION

The objective of this research was to formulate seismic source depth determination techniques, developed during this and two previous contracts, into an automated analysis procedure. The purpose is to substantially increase the percentage of events for which accurate source depths can be determined and to facilitate the analysis. In this procedure, the source depth is determined by the degree to which cepstrum patterns, computed from different portions of single or multistation seismic data, agree with those patterns expected for a given source depth. By automatically accounting for variations in the differential travel times caused by different station locations and the presence of later propagation modes, the depth phase information contained throughout the seismograms contribute to this depth estimate.

During this contract, the logic and algorithms necessary to incorporate and automate the various source depth analysis techniques were developed such that the seismic data and station to source distances are specified to obtain this source depth estimate. This work included the development of algorithms needed to store and access differential travel times as a function of source depth and station to source distances, for several different propagation modes.

The effectiveness of this automated source depth determination procedure was demonstrated through its application to the Illinois Event. The results of this analysis showed that the depth phase information, contained throughout the seismograms, was in fact

being constructively utilized and thereby enhanced the depth estimate. This was shown by obtaining the correct depth for this event through the separate analysis of the first and second minute of data verifying the usefulness of depth phase information contained in the later seismic propagation modes. A further verification was achieved by obtaining this depth estimate through the analysis of data arriving through individual propagation modes. In addition, it was shown that accurate depth estimates could be obtained from the analysis of data recorded at single stations. The primary result of these analyses is that unlike other analysis procedures, this automated seismic source depth determination procedure is utilizing depth phase information contained throughout the seismograms and should allow one to obtain accurate depth estimates for a higher percentage of events than previously possible.

During this contract, research was also conducted to investigate the effectiveness of these techniques in determining depths of shallow events; and to determine what modifications would enhance the analysis for this type of data. This research involved the analysis of both the Boxcar Event and synthesized shallow depth data.

2.0 AUTOMATED SEISMIC SOURCE DEPTH ANALYSIS

In order to both enhance and automate seismic source depth determinations, various techniques developed during this and two previous contracts, were formulated into a computerized procedure allowing the analyst to input seismic data and station to source epicenter distances to obtain a source depth estimate. In this procedure, the source depth is determined by the degree to which cepstrum patterns, computed from different portions of multi or single station seismic data, agree with those expected for a given source depth. The variations in differential travel time caused by the different station to source distances and the presence of later propagation modes are both accounted for and allow depth phase information contained throughout the seismogram to contribute to this depth estimate.

2.1 Seismic Source Depth Analysis Procedure

A prototype of the seismic source depth analysis procedure is flow charted in Figure 2.1. The input data consists of the seismic data recorded over a suite of stations, the data sample length (governing the maximum differential delay time observable), the length of coda to be analyzed, the offset times between the start of the data and the P-wave onset, and the station to source epicenter distances.

The automated analysis then proceeds to select a data sample from a given station recording and coda position and a cepstrum

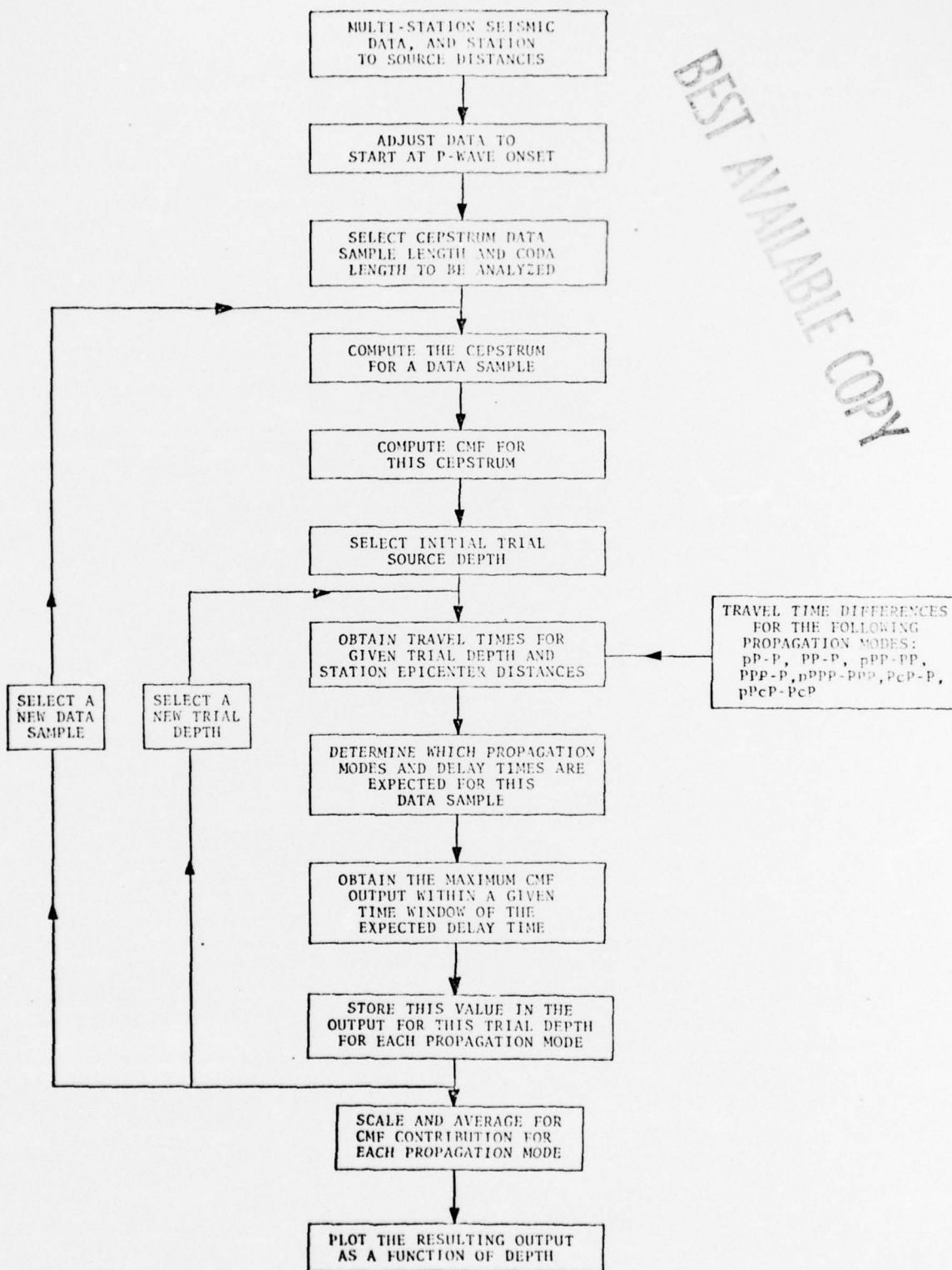


Figure 2.1. Seismic Source Depth Determination Procedure

and cepstrum matched filter (CMF) output is then computed from this data sample (Appendix A and Appendix B give details of the steps in computing the cepstrum and CMF). A flow chart of the CMF is shown in Figure 2.2. The first of a range of trial source depths is then selected. For this trial depth, and station to source epicenter distance, the differential travel time for the following propagation modes are accessed from computer storage: pP-P, PP-P, pPP-PP, PPP-P, pPPP-PPP, PcP-P, and pPcP-PcP. From the start and end time of the data sample, it is then decided which propagation modes will contribute to the CMF output for this particular data sample, and at what surface reflected delay times. The maximum CMF output within a given time window of this expected delay time is accumulated separately for each contributing propagation mode. For this same data sample, the procedure is repeated for each of the trial depths to be assumed. This completes the analysis of this data sample and the next sample is likewise processed. For each trial depth the CMF output is accumulated over the different data samples for each propagation mode. The accumulated CMF outputs for each propagation mode are then scaled and summed such that each mode has equal contribution and the final result is a plot of the cumulative CMF output versus depth. The cumulative CMF output versus depth for each propagation mode is also available as an optional output.

BEST AVAILABLE COPY

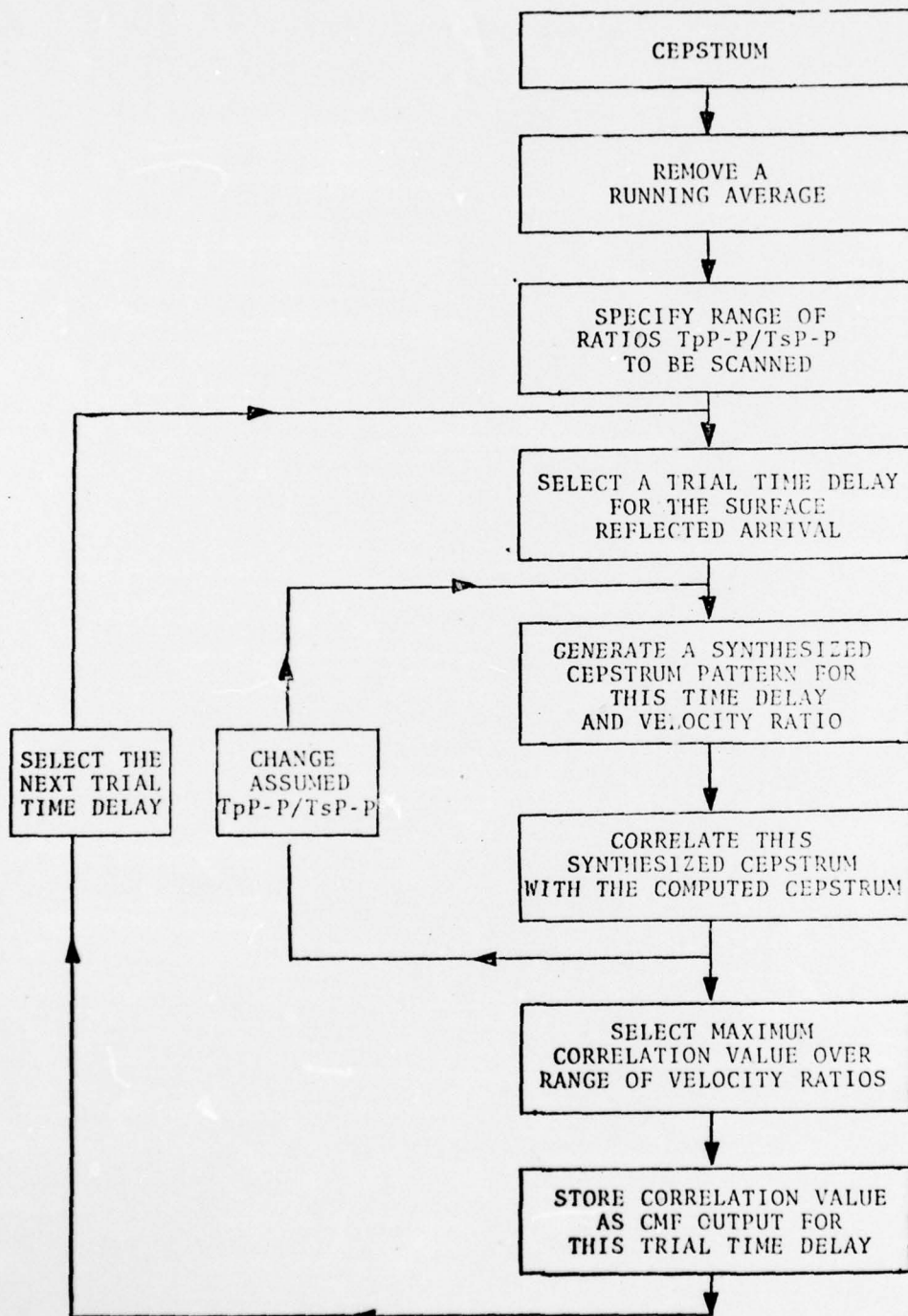


Figure 2.2. Calculation of Cepstrum Matched Filter (CMF) Output

2.2 Access and Storage of Differential Travel Time Information

In order to perform the automated source depth analysis one needs to determine which seismic propagation modes have arrived during a given data sample and what are the differential travel times between these arrivals and their associated surface reflections. For the event distances and depths of interest in this work the following seismic propagation modes are involved: pP-P, PP-P, pPP-PP, pPPP-PPP, PPP-P, pPcP-PcP and PcP-P. The automated analysis needs to access differential travel times for each of these propagation modes over the range of depths from 0 to 100 km and over epicenter distances of 10° to 90° to an accuracy of a few tenths of a second in most cases.

The travel time differences were obtained by the application of ray tracing using the spherically symmetric isotropic earth velocity model used for the BSSA seismological tables. A three dimensional polynomial surface representation of the differential travel time was used to facilitate computer access, reduce computer storage load and to perform the necessary interpolation of the computed values. We now describe the procedure used for obtaining the representation of the differential travel times as a function of source depth and source to receiver distance for the following seismic propagation modes: pP-P, PP-P, pPP-PP, PPP-P, pPPP-PPP, PcP-P and pPcP-PcP.

Case I: Surface Fits to pP-P, pPPP-PPP, pPP-PP, pPcP-PcP

An examination of Figure 2.1.1 suggests we represent these data as a double power series in which the travel time difference τ is the dependent variable and the depth d and epicenter distances Δ are the independent variables. The surface of travel time differences is then given by

$$\tau(d, \Delta) = \sum_{ij} \tau_{ij} \Delta^j d^i$$

The coefficients τ_{ij} and the number of them needed were determined as follows. Each curve at constant Δ_c was found to be adequately represented by a cubic in d :

$$\tau(d, \Delta_c) = \tau_1(\Delta_c)d + \tau_2(\Delta_c)d^2 + \tau_3(\Delta_c)d^3$$

Here τ vanishes at zero depth. The least squares values of $\tau_i(\Delta)$ were then in turn adjusted to a power series in Δ :

$$\tau_i(\Delta) = \sum_{j=0}^N \tau_{ij} \Delta^j, \quad i=1,2,3$$

Reliable input data for Δ less than 10° were not available, so no attempt was made to force $\tau_i(\Delta)$ to vanish at zero epicenter distance. Thus, our representation should be used only for $\Delta \geq 10^\circ$. All the data sets of Case I can be represented by $N=9$. Examples of the effectiveness of this representation are shown in Figures 2.1.2a through 2.1.2d for pP-P, pPP-PP, pPPP-PPP and pPcP-PcP.

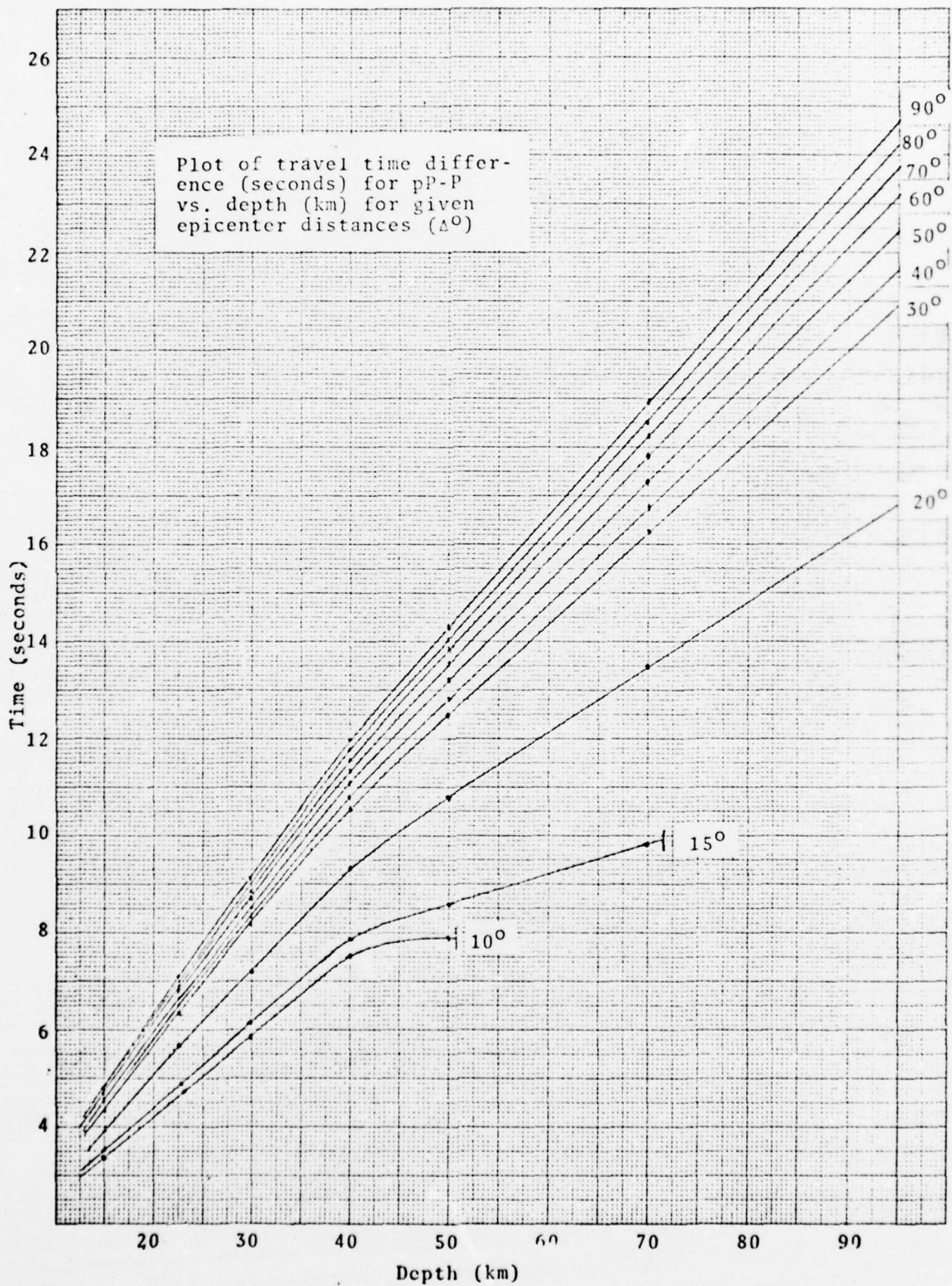


Figure 2.1.1
2-7

(P+)-P: TRAVEL TIME DIFF (SEC) VS DEPTH (KM) AND EPI-DISTANCE DELTA (DEG)

DOUBLE POWER SERIES COEFFICIENTS FOR CALCULATING TRAVEL TIME DIFFERENCE

	TAU SUB 1J	TAU SUB 2J	TAU SUB 3J
J = 0	.70451569E+00	-.88319599E-03	-.85335509E-04
J = 1	-.15119426E+00	.18381440E-02	-.78442494E-05
J = 2	.17816886E-01	-.35701456E-03	.31772821E-05
J = 3	-.10480308E-02	.27611793E-04	-.28151927E-06
J = 4	.36120111E-04	-.11502724E-05	.12401366E-07
J = 5	-.77702894E-06	.28589908E-07	-.31769065E-09
J = 6	.10590388E-07	-.43734706E-09	.49528985E-11
J = 7	-.89911917E-10	.40420244E-11	-.46377519E-13
J = 8	.42133363E-12	-.2071837E-13	.24000326E-15
J = 9	-.85973085E-15	.45239568E-16	-.52790138E-18

CALCULATED TRAVEL TIME DIFFERENCE TABLE

DELTA + DEPTH ↓	10.000	15.000	20.000	30.000	40.000	50.000	60.000	70.000	80.000	90.000
5.000	1.103	1.233	1.403	1.538	1.561	1.590	1.616	1.637	1.653	1.673
14.900	3.249	3.474	3.923	4.360	4.439	4.528	4.614	4.677	4.734	4.793
23.000	4.866	5.099	5.753	6.469	6.606	6.744	6.888	6.986	7.085	7.177
30.000	6.081	6.346	7.187	8.164	8.357	8.541	8.738	8.870	9.008	9.130
39.900	7.382	7.850	9.015	10.387	10.671	10.924	11.198	11.382	11.578	11.744
50.000	8.036	9.056	10.678	12.480	12.870	13.198	13.551	13.798	14.051	14.266
70.000	*****	10.405	13.556	16.262	16.891	17.397	17.885	18.296	18.637	18.962
100.000	*****	*****	17.527	21.622	22.670	23.533	24.102	24.906	25.245	25.784

RESIDUALS BETWEEN TRAVEL TIME DIFFERENCE INPUT AND CALCULATED TRAVEL TIME DIFFERENCE

DELTA + DEPTH ↓	10.000	15.000	20.000	30.000	40.000	50.000	60.000	70.000	80.000	90.000
5.000	.040	-.066	-.038	-.083	-.075	-.072	-.071	-.066	-.066	-.061
14.900	.125	.018	.010	-.008	.001	.002	-.001	.008	.011	.006
23.000	-.141	-.163	-.063	-.090	-.094	-.087	-.091	-.077	-.067	-.075
30.000	-.190	-.184	-.006	-.042	-.053	-.040	-.054	-.044	-.031	-.038
39.900	.156	.031	.305	.199	.156	.183	.145	.165	.173	.164
50.000	-.123	-.461	.069	.014	-.035	.002	-.027	.012	.009	.003
70.000	*****	-.587	-.046	-.009	-.120	-.083	-.087	-.085	-.027	-.053
100.000	*****	*****	.005	.231	-.069	-.082	.082	-.114	.151	.079

Figure 2.1.2a. Differential Travel Times Obtained from Polynomial Curve Fit for pp-p

BEST AVAILABLE COPY

(P+PP)-PP TRAVEL TIME DIFF (SEC) VS DEPTH (KM) AND EPI-DISTANCE DELTA (DEG)

DOUBLE POWER SERIES COEFFICIENTS FOR CALCULATING TRAVEL TIME DIFFERENCE

	TAU SUB 1J	TAU SUB 2J	TAU SUB 3J
J = 0	.1332966E+01	-.2458272E-01	.47856874E-03
J = 1	-.28393239E+00	.33328531E-02	-.74463907E-04
J = 2	.36372292E-01	-.90408566E-04	.29860351E-05
J = 3	-.18072171E-02	-.59734377E-05	.44096374E-07
J = 4	.65989127E-04	.46604204E-06	-.68787773E-08
J = 5	-.15259838E-05	-.13743890E-07	.23253861E-09
J = 6	.22355513E-07	.21990505E-09	-.40304687E-11
J = 7	-.24078632E-09	-.20139218E-11	.39346127E-13
J = 8	.12079121E-11	.99551033E-14	-.20598689E-15
J = 9	-.21645634E-14	-.20663571E-16	.45130638E-18

CALCULATED TRAVEL TIME DIFFERENCE TABLE (***** MEANS UNALLOWED DEPTH FOR GIVEN DELTA)

DELTA → DEPTH ↓	10.000	15.000	20.000	30.000	40.000	50.000	60.000	70.000	80.000	90.000
5.000	1.193	1.070	1.104	1.216	1.406	1.518	1.535	1.559	1.558	1.572
14.900	3.224	3.140	3.261	3.419	3.927	4.293	4.351	4.418	4.428	4.472
23.000	4.652	4.688	4.887	5.012	5.759	6.359	6.457	6.554	6.584	6.656
30.000	5.789	5.844	6.105	6.229	7.196	8.013	8.152	8.271	8.326	8.424
39.900	7.358	7.069	7.397	7.689	9.032	10.173	10.381	10.527	10.628	10.764
50.000	*****	7.665	8.915	8.849	10.711	12.195	12.490	12.658	12.816	12.994
70.000	*****	*****	*****	10.109	13.656	15.823	16.345	16.539	16.837	17.101
100.000	*****	*****	*****	*****	17.659	20.920	21.956	22.157	22.704	23.095

RESIDUALS BETWEEN TRAVEL TIME DIFFERENCE INPUT AND CALCULATED TRAVEL TIME DIFFERENCE

DELTA → DEPTH ↓	10.000	15.000	20.000	30.000	40.000	50.000	60.000	70.000	80.000	90.000
5.000	-.083	.047	.043	-.055	-.077	-.077	-.081	-.078	-.075	-.069
14.900	.093	.201	.115	.056	.012	-.012	-.007	-.022	.014	.014
23.000	.021	.001	-.156	-.097	-.064	-.094	-.066	-.111	-.073	-.067
30.000	.031	.002	-.201	-.086	-.017	-.048	-.038	-.059	-.024	-.028
39.900	.080	.404	.141	.183	.301	.207	.203	.170	.201	.215
50.000	*****	.102	-.120	-.252	.931	.027	.003	-.004	.013	.022
70.000	*****	*****	*****	-.288	-.141	-.004	-.100	-.130	-.069	-.062
100.000	*****	*****	*****	*****	-.260	.256	-.108	.032	-.101	-.052

Figure 2.1.2b. Differential Travel Times Obtained from Polynomial Curve Fit for PPP-PP

BEST AVAILABLE COPY

(P+P)PPP TRAVEL TIME DIFF (SEC) VS DEPTH (KM) AND EPI-DISTANCE DELTA (DEG)

DOUBLE POWER SERIES COEFFICIENTS FOR CALCULATING TRAVEL TIME DIFFERENCE

	TAU SUR 1J	TAU SUR 2J	TAU SUR 3J
J = 0	-.77633889E+00	.68361173E-01	-.13622038E-02
J = 1	.29864625E+00	-.20124183E-01	.38960040E-03
J = 2	-.34221106E-01	.22266622E-02	-.42768587E-04
J = 3	.20635643E-02	-.12835418E-03	.24445225E-05
J = 4	-.74268357E-04	.44007204E-05	-.82830884E-07
J = 5	.16826877E-05	-.95205747E-07	.17628515E-08
J = 6	-.24211801E-07	.13166893E-08	-.23880077E-10
J = 7	.21451030E-09	-.11306496E-10	.20021912E-12
J = 8	-.16663313E-11	.54928750E-13	-.94807249E-15
J = 9	.22742755E-14	-.11533281E-15	.19392923E-17

CALCULATED TRAVEL TIME DIFFERENCE TABLE

DELTA → DEPTH ↓	10.000	15.000	20.000	30.000	40.000	50.000	60.000	70.000	80.000	90.000
5.000	1.207	1.173	1.140	1.100	1.194	1.327	1.443	1.485	1.528	1.540
14.900	3.252	3.242	3.210	3.257	3.343	3.639	4.012	4.203	4.321	4.354
23.000	4.679	4.732	4.811	4.890	4.878	5.249	5.862	6.229	6.400	6.447
30.000	5.806	5.911	6.022	6.117	6.034	6.458	7.302	7.851	8.067	8.124
39.900	7.345	7.405	7.342	7.423	7.384	7.913	9.125	9.965	10.248	10.319
50.000	*****	*****	*****	*****	8.399	9.135	10.778	11.938	12.301	12.386
70.000	*****	*****	*****	*****	9.250	10.975	13.656	15.436	16.028	16.146
100.000	*****	*****	*****	*****	*****	13.039	17.815	20.191	21.429	21.635

RESIDUALS BETWEEN TRAVEL TIME DIFFERENCE INPUT AND CALCULATED TRAVEL TIME DIFFERENCE

DELTA → DEPTH ↓	10.000	15.000	20.000	30.000	40.000	50.000	60.000	70.000	80.000	90.000
5.000	-.080	-.073	.032	.052	-.052	-.122	-.118	-.068	-.072	-.088
14.900	.087	.063	.120	.114	.059	-.027	.012	.011	.010	-.005
23.000	-.003	-.064	-.138	-.155	-.097	-.120	-.052	-.096	-.060	-.074
30.000	.012	-.100	-.197	-.215	-.064	-.025	-.074	-.060	-.002	-.018
39.900	.069	-.049	.113	.126	.279	.351	.185	.151	.251	.258
50.000	*****	*****	*****	-.173	-.236	.067	-.035	-.059	.093	.103
70.000	*****	*****	*****	*****	-.210	-.002	-.130	-.133	.063	.019
100.000	*****	*****	*****	*****	*****	.430	-.201	-.144	.173	.191

Figure 2.1.2c. Differential Travel Times Obtained from Polynomial Curve Fit for pppp-ppp

BEST AVAILABLE COPY

(P+)-PCP-PCP TRAVEL TIME DIFF (SEC) VS DEPTH (KM) AND EPI-DISTANCE DELTA (DEG)

DOUBLE POWER SERIES COEFFICIENTS FOR CALCULATING TRAVEL TIME DIFFERENCE

	TAU SUR 1J	TAU SUR 2J	TAU SUR 3J
J = 0	.43430116E+00	-.39806067E-02	.26096260E-04
J = 1	-.14028699E-01	.72844003E-03	-.55860908E-05
J = 2	.14257720E-02	-.78747384E-04	.59120923E-06
J = 3	-.71953567E-04	.43250873E-05	-.31612775E-07
J = 4	.19617097E-05	-.13472496E-06	.94863732E-09
J = 5	-.28743273E-07	.24805786E-08	-.16505101E-10
J = 6	.18608125E-09	-.26787129E-10	.16162892E-12
J = 7	.25233836E-12	.15802061E-12	-.76825728E-15
J = 8	-.97609346E-14	-.40814595E-15	.70592439E-18
J = 9	.36591070E-16	.12450430E-18	.45708095E-20

CALCULATED TRAVEL TIME DIFFERENCE TABLE (***** MEANS UNALLOWED DEPTH FOR GIVEN DELTA)

DELTA → DEPTH ↓	10.000	15.000	20.000	30.000	40.000	50.000	60.000	70.000	80.000	90.000
5.00	1.724	1.723	1.726	1.715	1.703	1.699	1.691	1.679	1.682	1.683
14.90	4.953	4.947	4.948	4.921	4.887	4.870	4.848	4.819	4.821	4.823
23.00	7.431	7.419	7.413	7.376	7.325	7.293	7.263	7.224	7.219	7.221
30.00	9.469	9.449	9.434	9.392	9.326	9.279	9.243	9.198	9.184	9.185
39.90	12.216	12.179	12.148	12.099	12.013	11.942	11.900	11.846	11.817	11.817
50.00	14.869	14.825	14.777	14.720	14.613	14.516	14.469	14.404	14.358	14.356
70.00	19.862	19.788	19.716	19.637	19.477	19.338	19.274	19.172	19.099	19.094
100.00	27.187	27.073	27.028	26.864	26.583	26.432	26.306	26.075	26.012	26.007

RESIDUALS BETWEEN TRAVEL TIME DIFFERENCE INPUT AND CALCULATED TRAVEL TIME DIFFERENCE

DELTA → DEPTH ↓	10.000	15.000	20.000	30.000	40.000	50.000	60.000	70.000	80.000	90.000
5.00	-.059	-.058	-.066	-.063	-.057	-.064	-.056	-.049	-.058	-.050
14.90	.009	.007	-.004	-.001	.010	-.000	.009	.024	.019	.016
23.00	-.072	-.070	-.080	-.080	-.071	-.077	-.079	-.061	-.071	-.079
30.00	-.038	-.034	-.041	-.048	-.040	-.043	-.049	-.035	-.036	-.048
39.90	.149	.158	.161	.144	.154	.151	.145	.158	.168	.165
50.00	-.003	.013	.021	-.014	-.005	-.002	-.027	-.009	.005	-.002
70.00	-.056	-.024	-.047	-.068	-.051	-.076	-.092	.005	-.042	-.054
100.00	.004	.058	.019	-.023	.038	-.014	-.050	.064	.058	.024

Figure 2.1.2d. Differential Travel Times Obtained from Polynomial Curve Fit for pcp-pcp

BEST AVAILABLE COPY

Each differential travel time surface considered in this work, except those representing core reflections, exhibit an unallowed region, i.e., there exists a range of epicenter distances for which below a certain depth the surface reflected mode is not received. The boundary of such a region projected into the (d, Δ) plane for pP-P is shown in Figure 2.1.3.

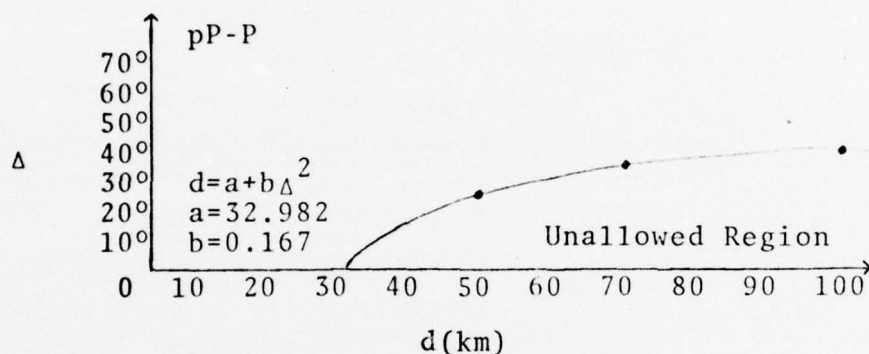


Figure 2.1.3

These boundaries can be adequately represented by a parabola so that our polynomial model is subject to the constraint that for a given Δ we must have $d < a + b\Delta^2$, where a and b have been determined from least square adjustments to plots like that of Figure 2.1.3. In Figure 2.1.2 the unallowed region is shown as asterisk table entries.

Case II: Line Fits to PP-P, PPP-P, PcP-P

These travel time difference plots can be represented as single curves depending on Δ only, since between 5 and 100 km, the depth dependence is very weak. Thus we have

$$\tau(d, \Delta) = \tau_o(\Delta) = \sum_{j=0} \tau_{oj} \Delta^j.$$

The PP-P and PPP-P differences appear to vanish as $\Delta \rightarrow 0$, so for these curves we set $\tau_{oo} = 0$ and also find $N=8$ is sufficient. For PcP-P, the core reflection insures that $\tau_{oo} \neq 0$. Here $N=6$ is sufficient.

This polynomial surface representation of the differential travel times can be stored using a total of 143 coefficients and requires less than .02 seconds to compute these times for eight propagation modes on the CDC 6600 computer.

3.0 APPLICATION OF THE ANALYSIS PROCEDURE TO THE ILLINOIS EVENT

In order to establish that this automated analysis procedure was in fact constructively utilizing depth phase information throughout the seismic coda and thereby enhancing one's ability to extract accurate source depth estimates, the Illinois Event was analyzed in several ways. Although depth phase delay times can be obtained using conventional procedures for this event by demonstrating that these delay times can be obtained using only the coda of the event, individual stations, data arriving through individual propagation modes, and portions of the data for which conventional analysis fails, we can demonstrate that this new procedure extracts and properly interprets considerably more depth phase information than previous methods. The ability to accomplish this will enable seismic source depth determinations for events having poorer signal/noise ratios and/or recorded at fewer stations than was previously possible.

In Figure 3.1 are plotted the first portion of the seismograms recorded from the Illinois Event of 11/9/68. To appreciate what this automated analysis procedure must accomplish consider Figure 3.2. Here are plotted 19 cepstrums computed from consecutive 12.8 second data samples along the seismogram recorded at WHZYK. This shows complex and changing cepstrum patterns, most of which contain depth phase information which must be constructively utilized. This is primarily accomplished using the cepstrum matched filter technique in conjunction with differential travel time information for several propagation modes.

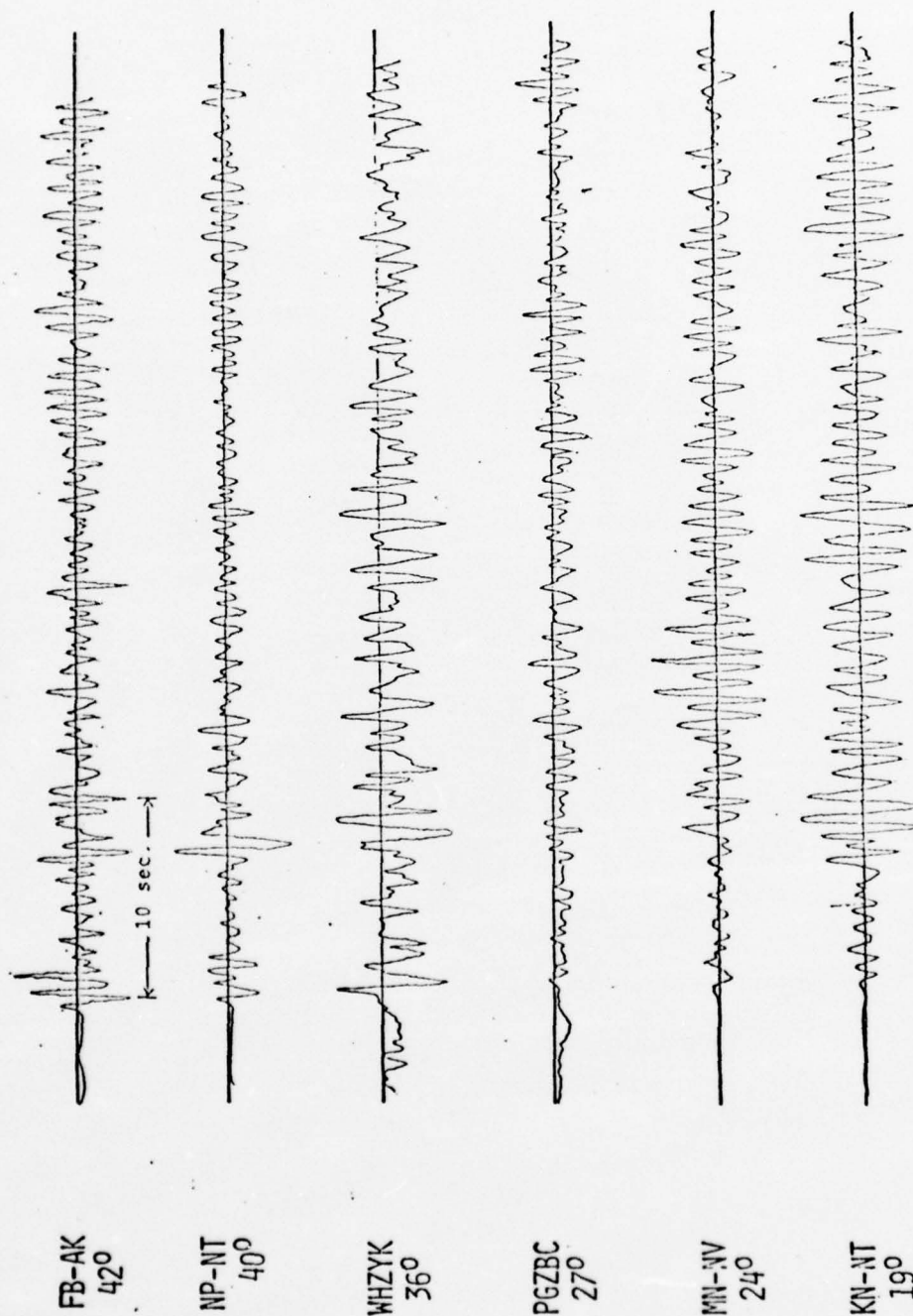
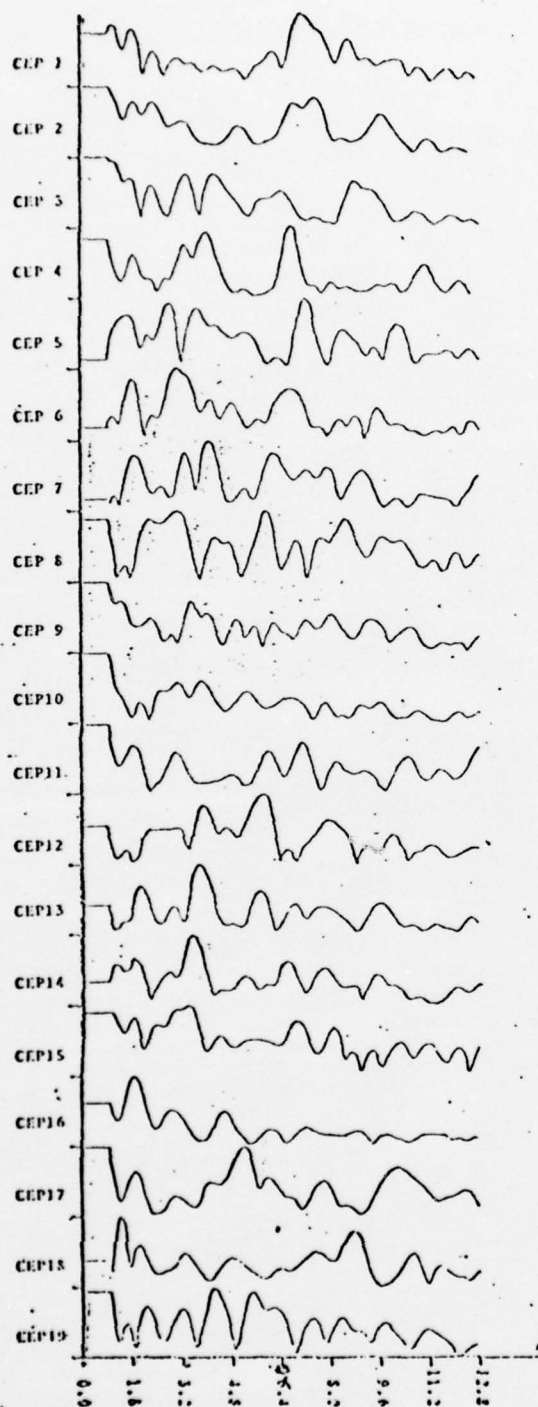


Figure 3.1



Cepstra Calculated for Consecutive
12.8 Second Data Samples Along Gode
(50% Sample Overlap) for Illinois
Event Station 1821A.

Figure 3.2

The Illinois Event was first analyzed using the first two minutes of data recorded at all six stations. The output of the automated analysis is plotted in Figure 3.3 as cumulative CMF output versus depth in km. The result is a very clear dominant peak indicating the correct source depth of 26 ± 2 km for this event. However, a more impressive result is seen in Figure 3.4. Here the same analysis was performed using only the second minute of data and again a clear detection of the event depth is obtained. Through the omission of the first minute of data we have allowed only the later propagation modes (PP, PPP, PcP) to contribute to this result and have clearly demonstrated that this analysis procedure is indeed constructively utilizing depth phase information normally ignored.

Another way of showing that depth phase information, arriving in the later seismic propagation modes is contributing to the source depth estimate, is to compute the CMF output versus depth for the data arriving from individual propagation modes. In Figure 3.5a through 3.5d are the analysis results for the P, PP, PPP and PcP modes individually processed using two minutes of data from each of six stations. In each of these plots a clear detection of the correct depth is obtained.

The ability of this analysis procedure to utilize the differential travel times information of later propagation modes has another important advantage. That is, a major improvement in the ability to obtain seismic source depths from data recorded at a single station. The reason is that normally one requires that there be moveout in the depth phase delay times over a suite of stations in order to be confident that the depth phase has been detected. However, in this new analysis procedure,

CUMULATIVE CMF OUTPUT VERSUS DEPTH USING 2 MINUTES OF DATA
FOR ALL SIX STATIONS FOR ALL MODES COMBINED (ILLINOIS EVENT)

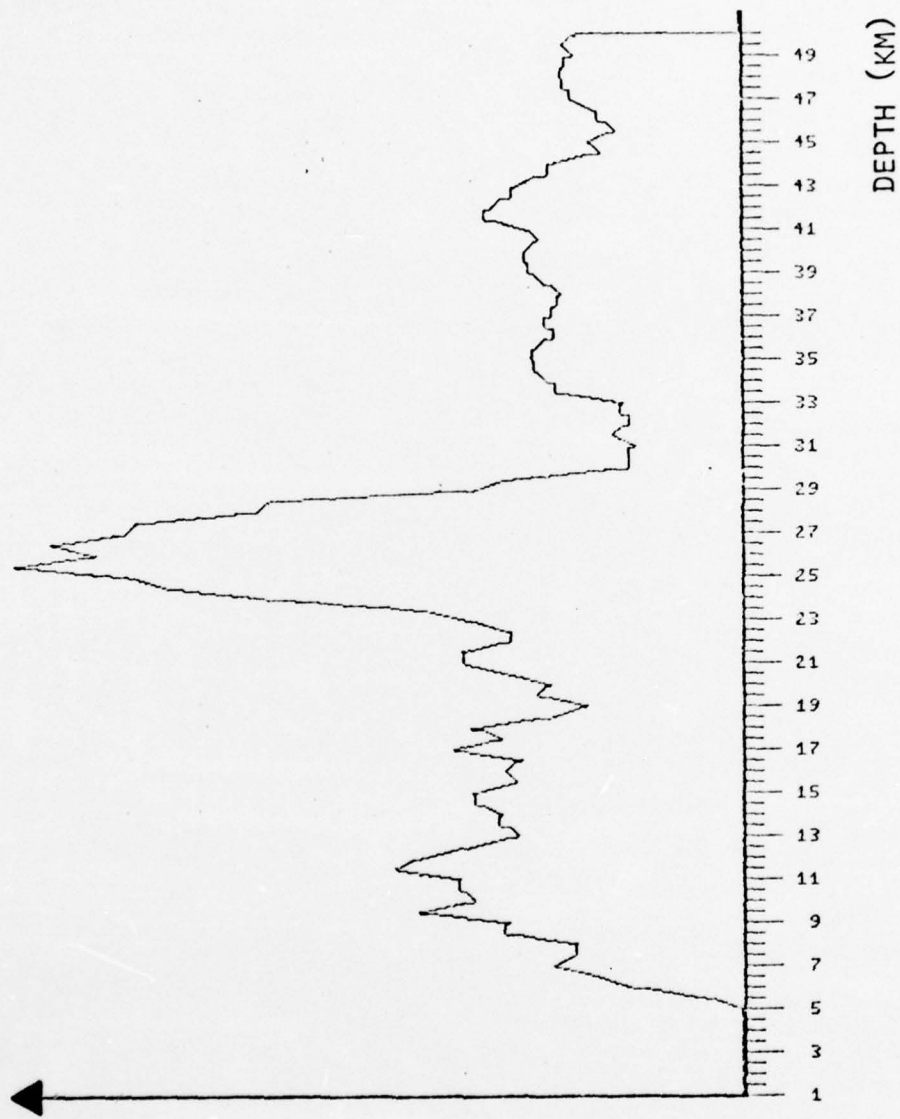


Figure 3.3

CUMULATIVE CMF OUTPUT VERSUS DEPTH USING ONLY THE 2ND
MINUTE OF DATA FROM ALL SIX STATIONS (ILLINOIS EVENT)

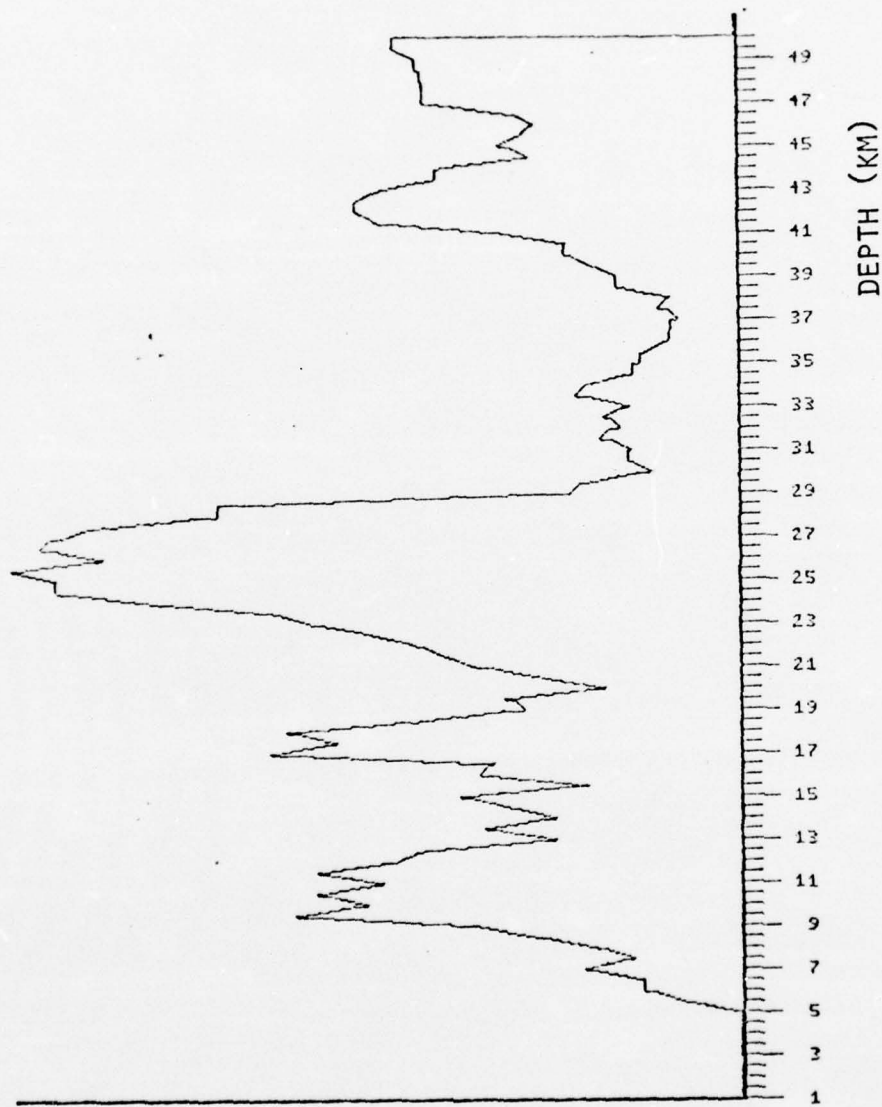


Figure 3.4

CMF OUTPUT VERSUS DEPTH USING 2 MINUTES OF DATA FOR ALL
SIX STATIONS FOR P MODE ONLY (ILLINOIS EVENT)

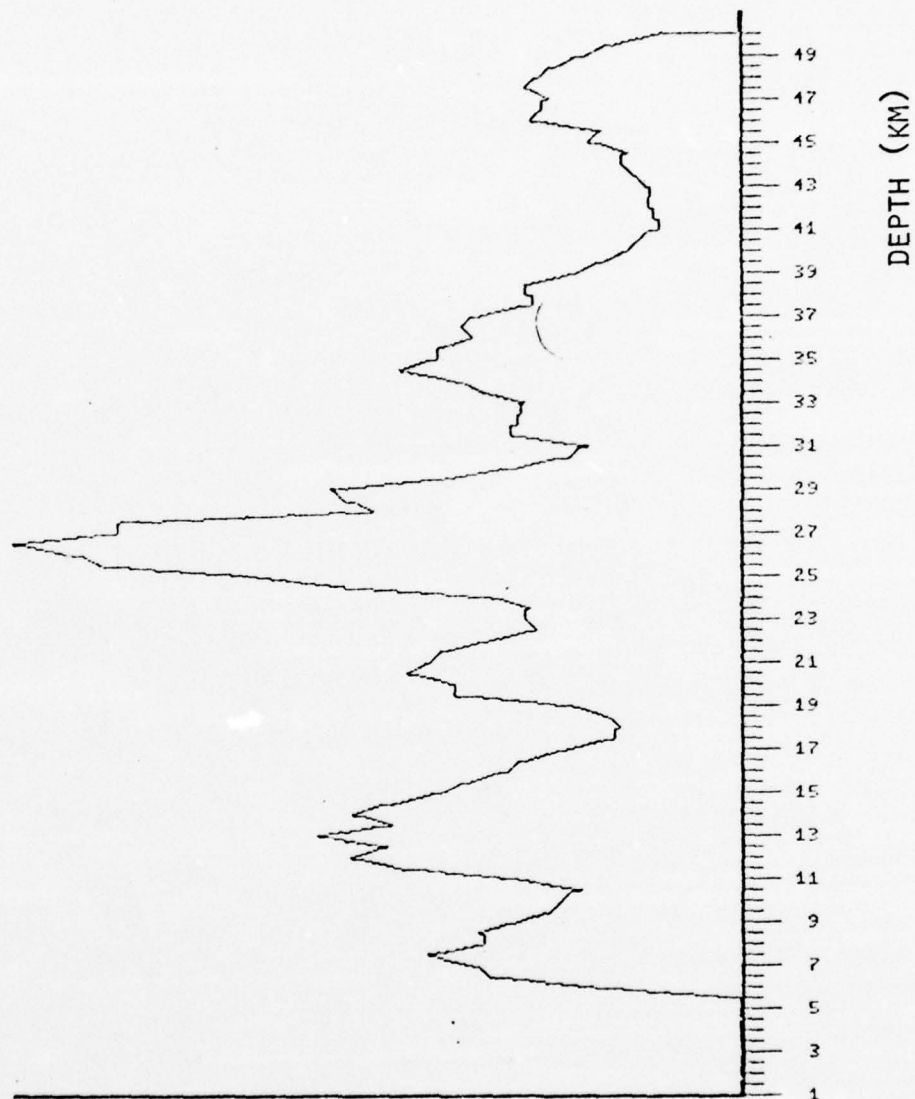


Figure 3.5a

CMF OUTPUT VERSUS DEPTH USING 2 MINUTES OF DATA FOR ALL
SIX STATIONS FOR PP MODE ONLY (ILLINOIS EVENT)

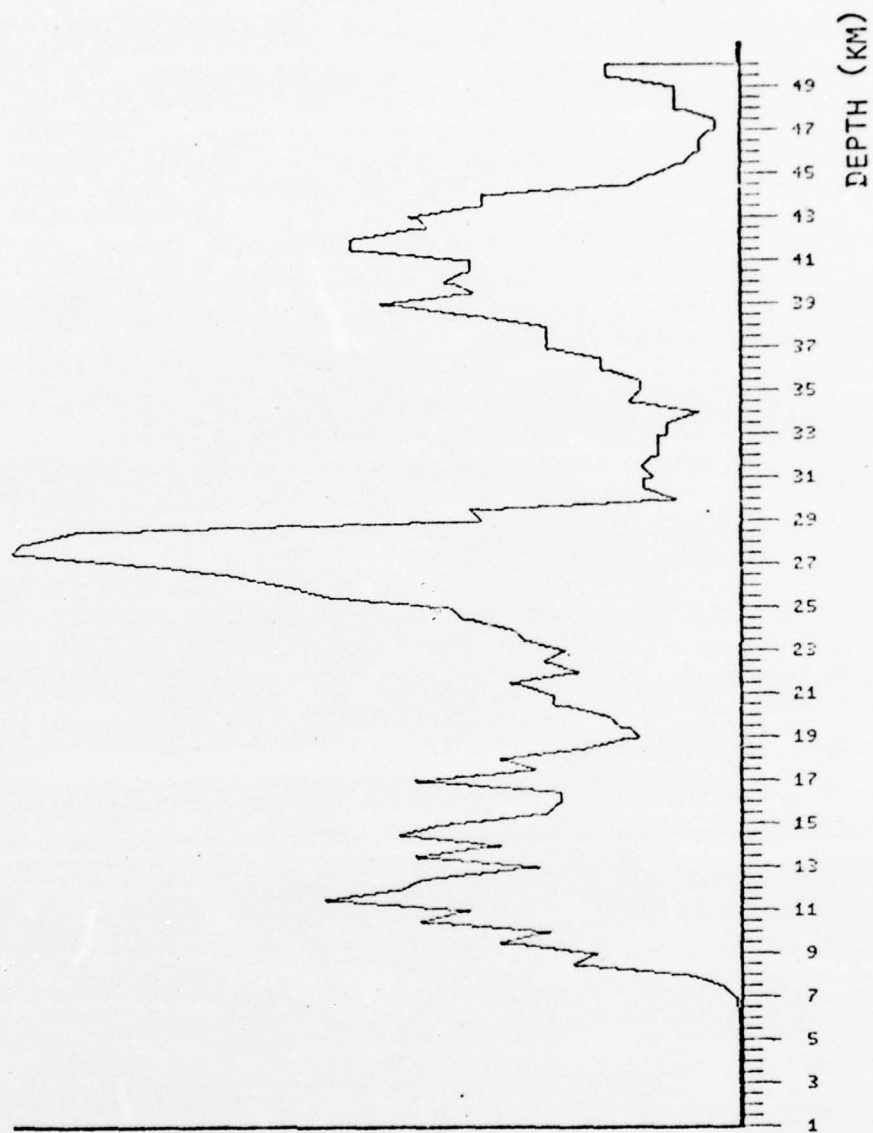


Figure 3.5b

CMF OUTPUT VERSUS DEPTH USING 2 MINUTES OF DATA FOR ALL
SIX STATIONS FOR PPP MODE ONLY (ILLINOIS EVENT)

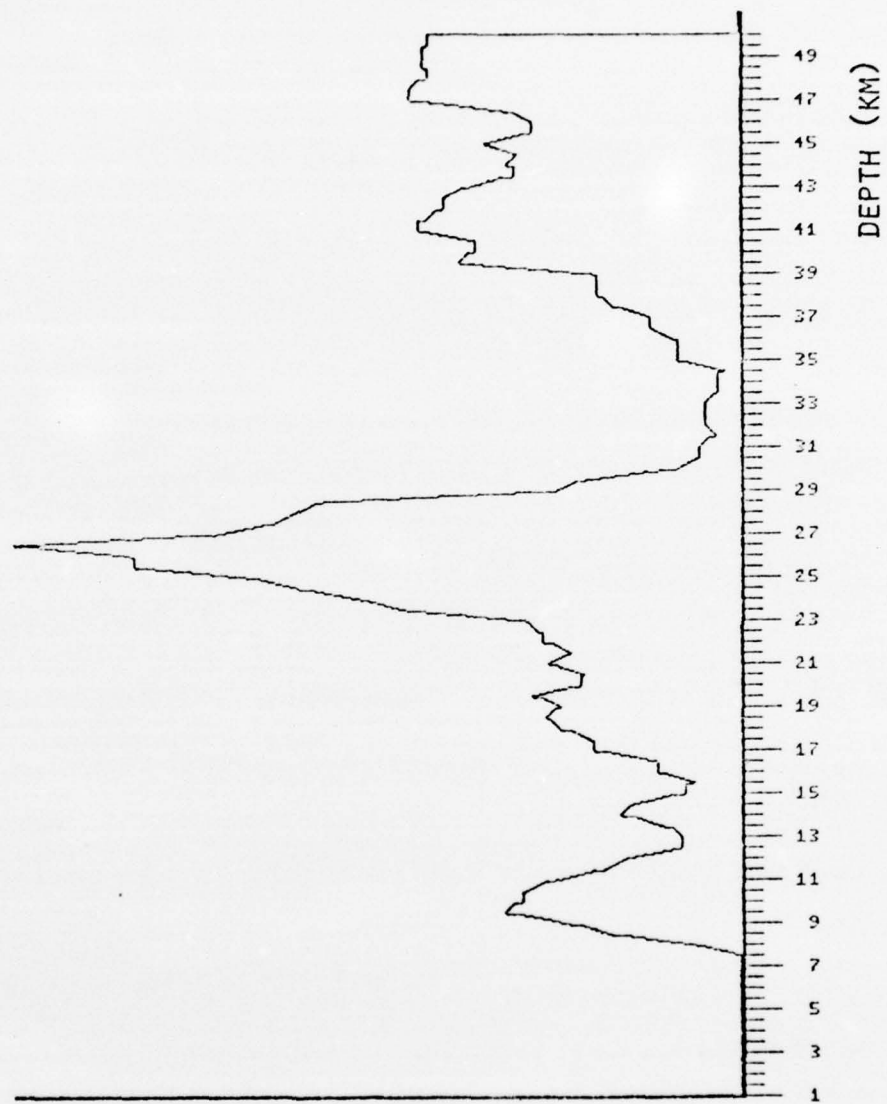


Figure 3.5c

CMF OUTPUT VERSUS DEPTH USING 2 MINUTES OF DATA FOR ALL
SIX STATIONS FOR PCP MODE ONLY (ILLINOIS EVENT)

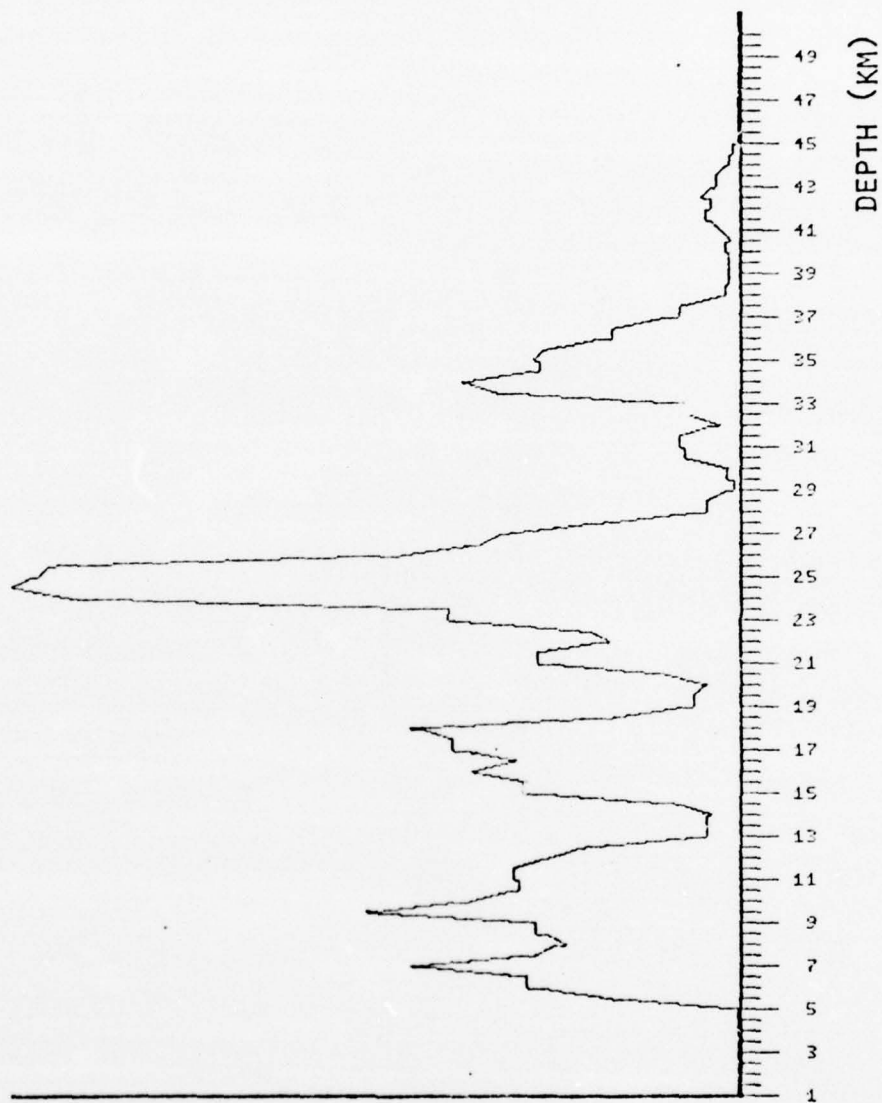


Figure 3.5d

depth phase delay time moveout occurs along the coda, as different propagation modes contribute, as well as between stations. Thus, the final CMF output versus depth obtained from the analysis of a data recorded at a given station, reflects the degree to which the various delay times are in agreement with a given source depth.

In Figure 3.6a through 3.6f are the CMF outputs, using one minute of data, from the individual analysis of data recorded at KN-UT, MN-NV, PGZBC, WHZYK, NP-NT and FB-AK. As can be seen from these figures, in all but the closest station KN-UT, the automated analysis procedure gives very good indications of a ~26 km source depth through the analysis of data recorded at an individual station. Such a capability is very important since many small magnitude events will only be recorded on very few stations.

From the analysis of the Illinois Event using this new automated seismic source depth determination procedure, all indications are that the concepts and techniques used in the analysis are valid and that substantial increases in the percentage of deeper events (>5 km) for which source depths can be established should be realized.

In the next section we discuss the applicability of these techniques to shallow events.

CMF OUTPUT VERSUS DEPTH USING 1 MINUTE OF DATA
RECORDED AT STATION KN-UT (ILLINOIS EVENT)

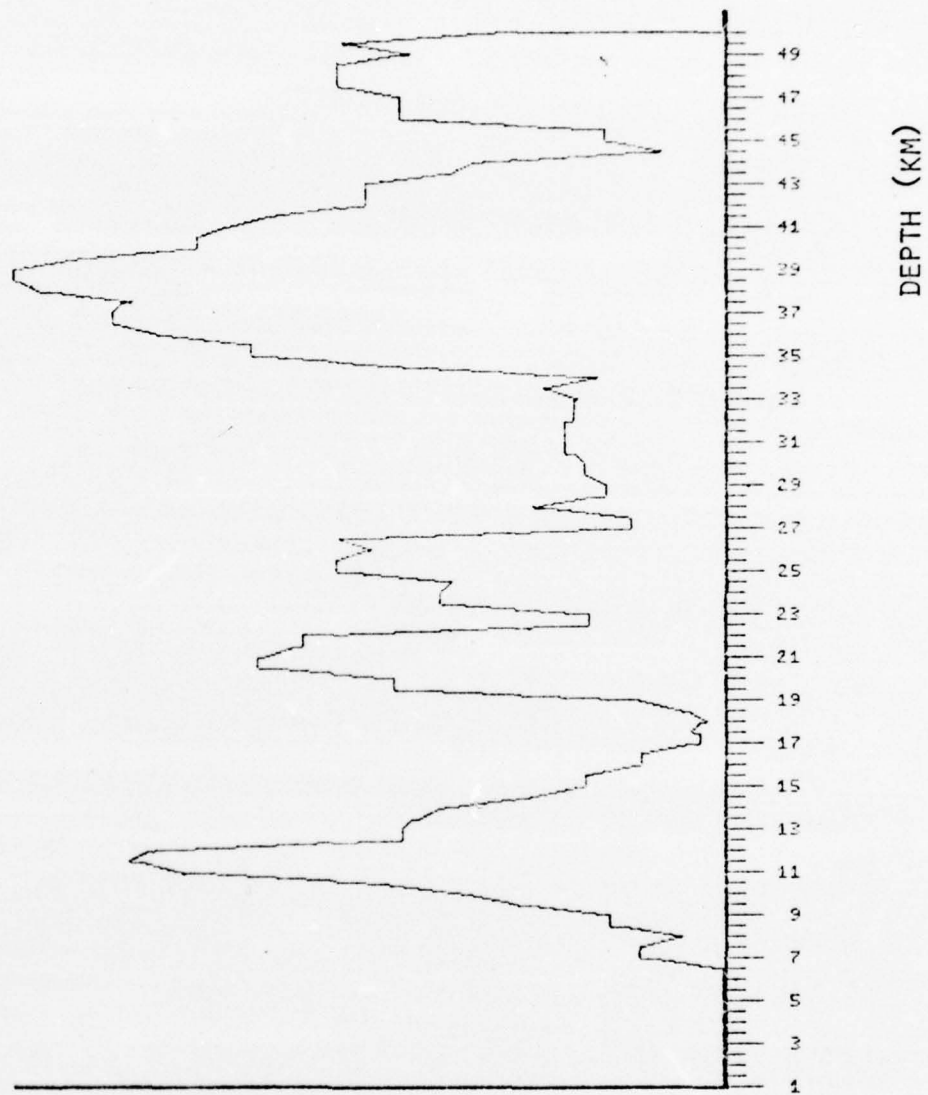


Figure 3.6a

CMF OUTPUT VERSUS DEPTH USING 1 MINUTE OF DATA
RECORDED AT STATION MN-NV (ILLINOIS EVENT)

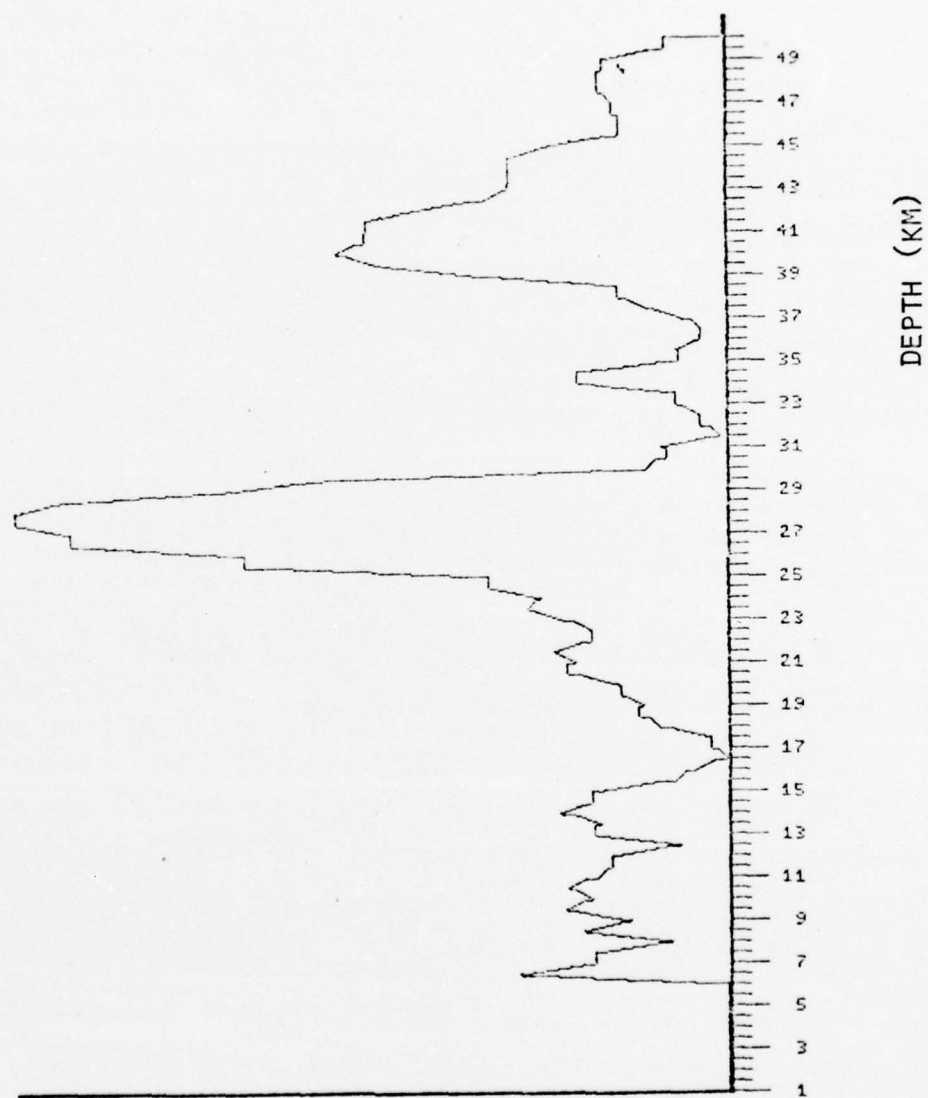


Figure 3.6b

CMF OUTPUT VERSUS DEPTH USING 1 MINUTE OF DATA
RECORDED AT STATION PGZBC (ILLINOIS EVENT)

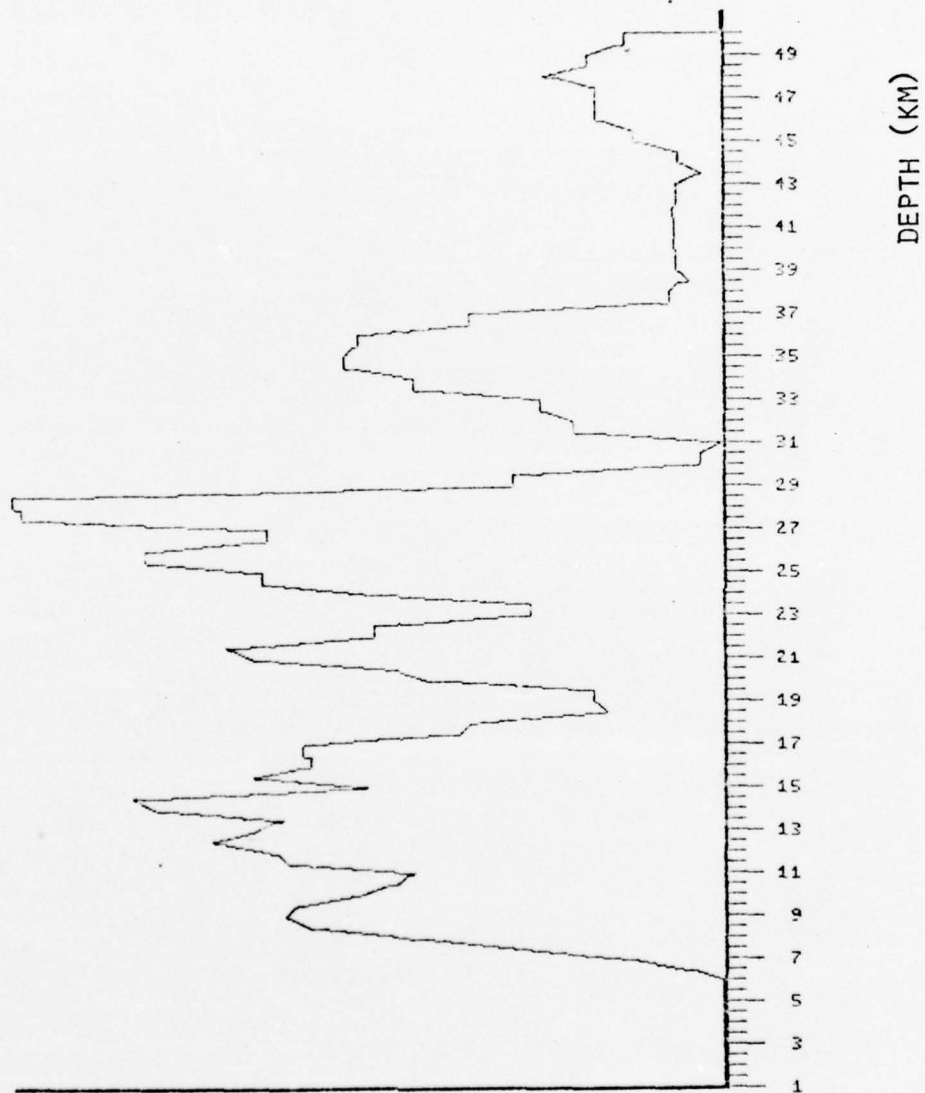


Figure 3.6c

CMF OUTPUT VERSUS DEPTH USING 1 MINUTE OF DATA
RECORDED AT STATION WHZYK (ILLINOIS EVENT)

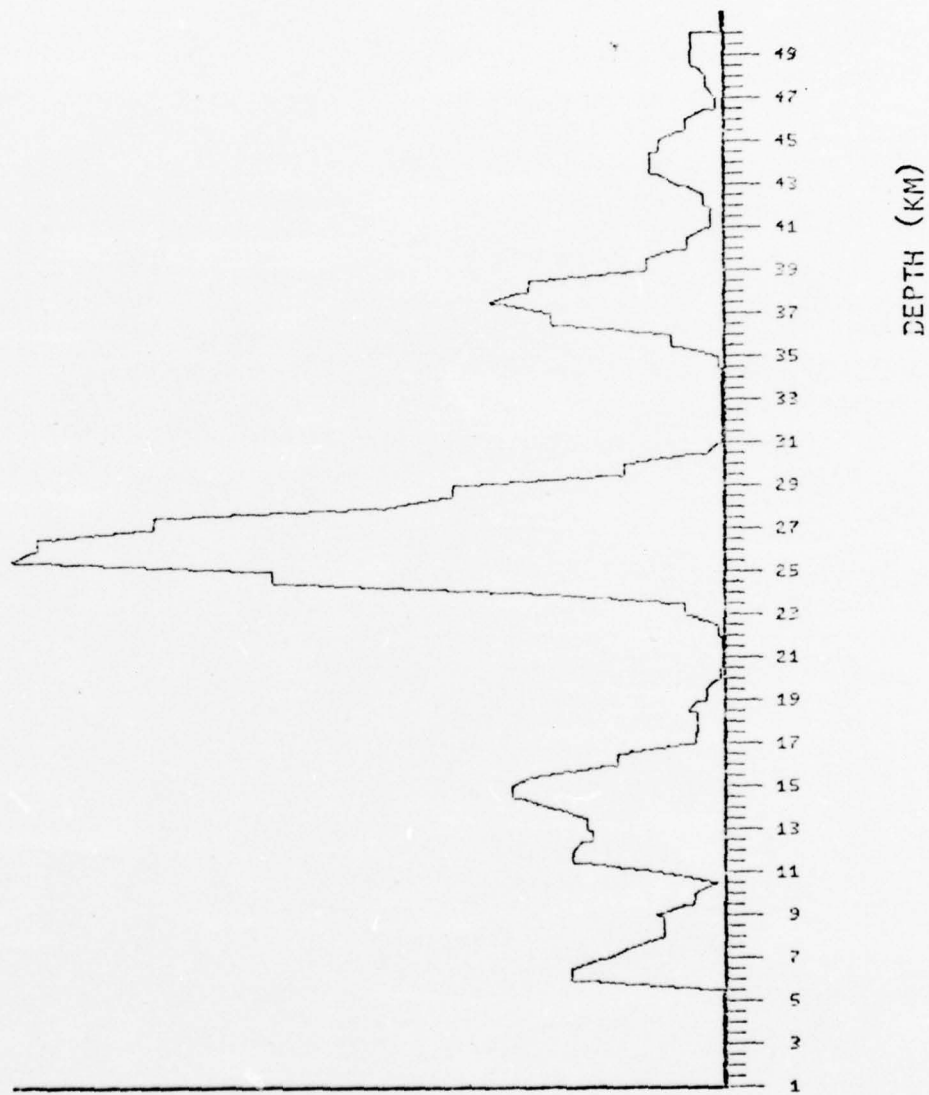


Figure 3.6d

CMF OUTPUT VERSUS DEPTH USING 1 MINUTE OF DATA
RECORDED AT STATION NP-NT (ILLINOIS EVENT)

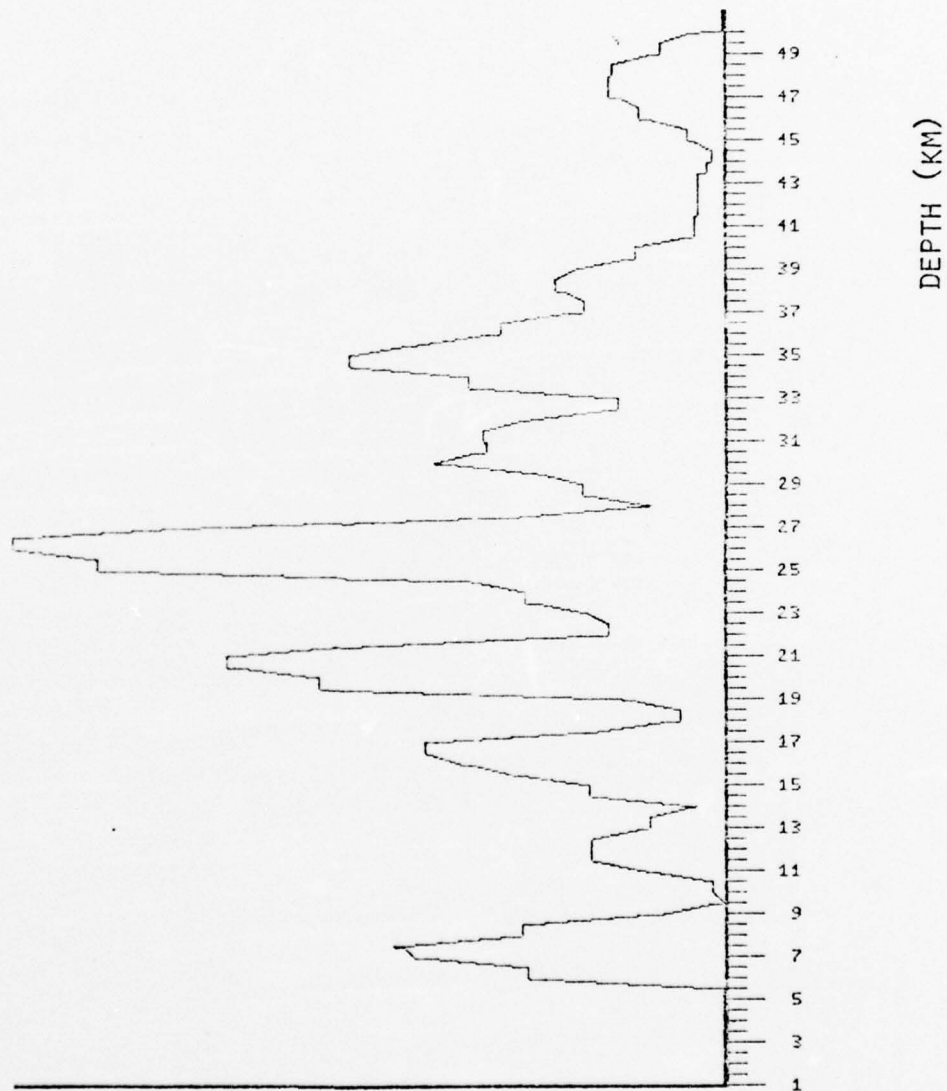


Figure 3.6e

CMF OUTPUT VERSUS DEPTH USING 1 MINUTE OF DATA
RECORDED AT STATION FB-AK (ILLINOIS EVENT)

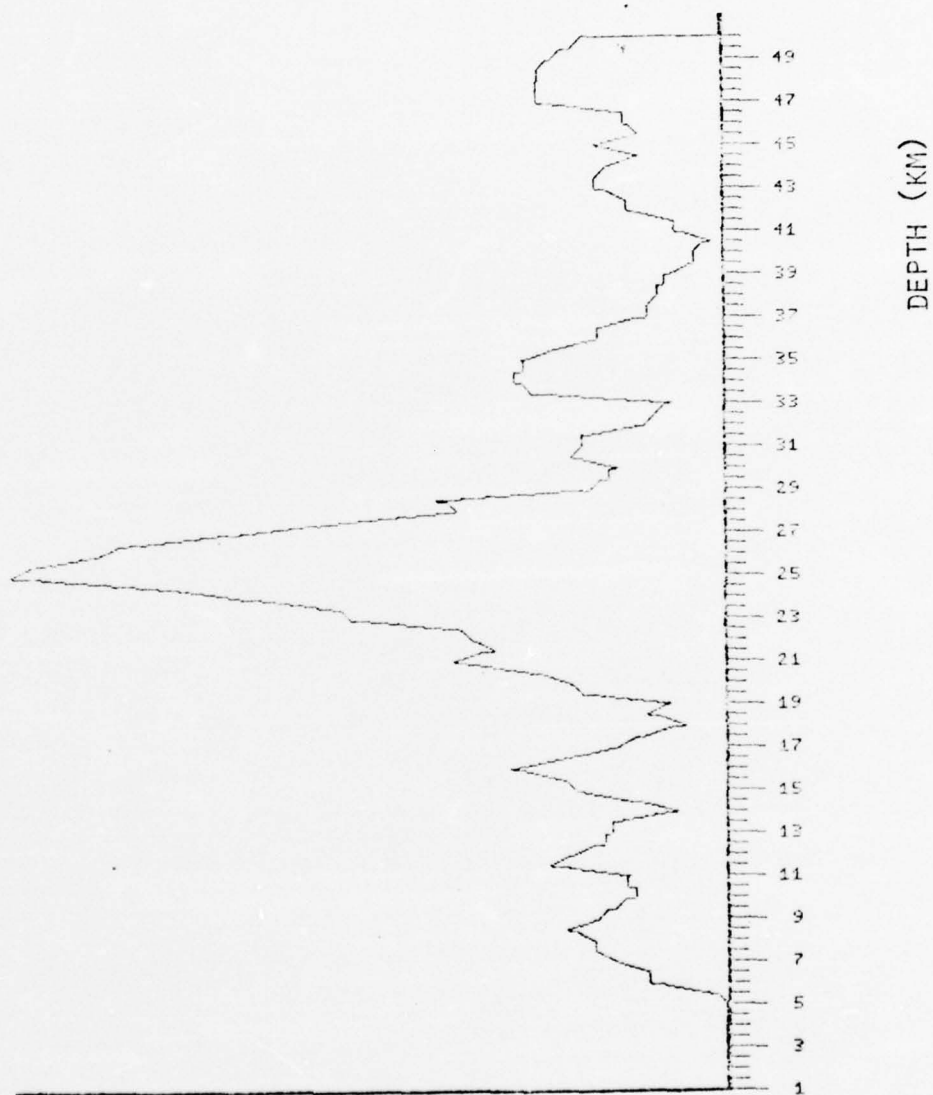


Figure 3.6f

4.0 SHALLOW SOURCE DEPTH DETERMINATION USING CEPSTRUM ANALYSIS

In order to apply cepstrum analysis to the problem of determining delay times of surface reflected seismic energy for shallow source depths (<5 km), one faces the problem of short delay times (<1 sec) relative to the available signal bandwidth (.5-3 Hz). As a consequence, the modulation of the spectrum contains less than a few cycles and becomes difficult to distinguish from the power spectrum of seismic arrivals not containing surface reflections.

In order to determine the effectiveness of the automated analysis and to shed some light on possible improvements and limits of cepstrum analysis for these shallow depths, we analyzed both real and synthesized seismic data. This included the analysis of the Boxcar Event, known to be at a depth of 1.12 km, and the Illinois Event having a source depth of ~ 26 km for the purpose of comparison. This analysis was done using the automated analysis procedure modified for short delay times by the removal of spectral tapering and the cepstrum matched filter (not effective in its present form for shallow depths) and by increasing the interpolation of the cepstrum.

4.1 Analysis of the Boxcar Event

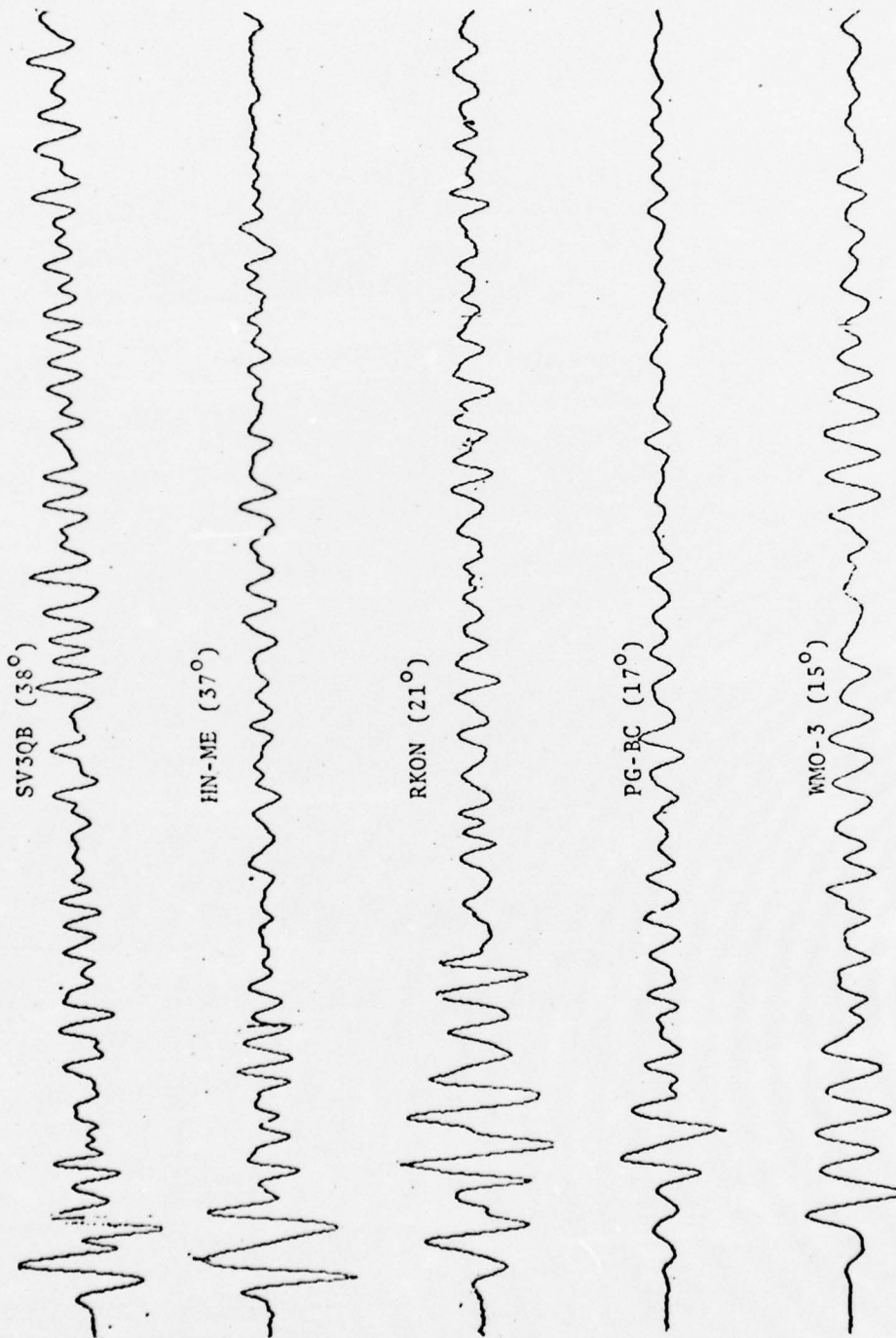
Analysis of the Boxcar Event was done using data recorded at five stations having epicenter distances of 15° , 17° , 21° , 37° and 38° . Seven 12.8 second consecutive data samples from

each station recording were used in the analysis. The first 50 seconds of these seismograms are plotted in Figure 4.1.1a. Figure 4.1.1b is a plot of the averaged amplitude spectrum for the 35 Boxcar time samples over the frequency range 0-2.5 Hz.

We see that we are dealing with a fairly narrow band signal which in effect can be considered to have a half cycle modulation in the amplitude spectrum. Figure 4.1.2 is the plot of the cumulative CMF output versus depth in km resulting from the modified automated analysis of the Boxcar Event. This result shows little more than an inflection in the vicinity of the known depth of 1.12 km. However, if one computes the cepstrum using Maximum Entropy spectral analysis for the transform of the amplitude spectrum, the results of Figure 4.1.3 show a definite peak in the 1.1 km range. This occurs since Maximum Entropy spectral analysis is known to be more effective at obtaining magnitudes of frequency components when less than a few cycles are present. One variable in this procedure is the filter length which we settled on 125 out of a sample containing 256 points.

The peak at ~1.1 km appears to be a very encouraging result; however, we must remember that the shape of the narrow band source spectrum itself can introduce structure in the cepstrum at these short delay times. We, therefore, performed the identical analysis (using Maximum Entropy) on the Illinois Event known to be at a greater depth and having a somewhat similar amplitude spectrum as seen in Figure 4.1.4. The result of this analysis, shown in Figure 4.1.5, shows an inflection at the 1.1 km depth range and together with the results of the CMF output for the PP mode seen in Figure 4.1.6, one sees that the spectral shape can indeed introduce such features and the results of the Boxcar analysis must be interpreted with this in mind.

BOXCAR EVENT



4-3

← 10 sec. →

Figure 4.1.1a

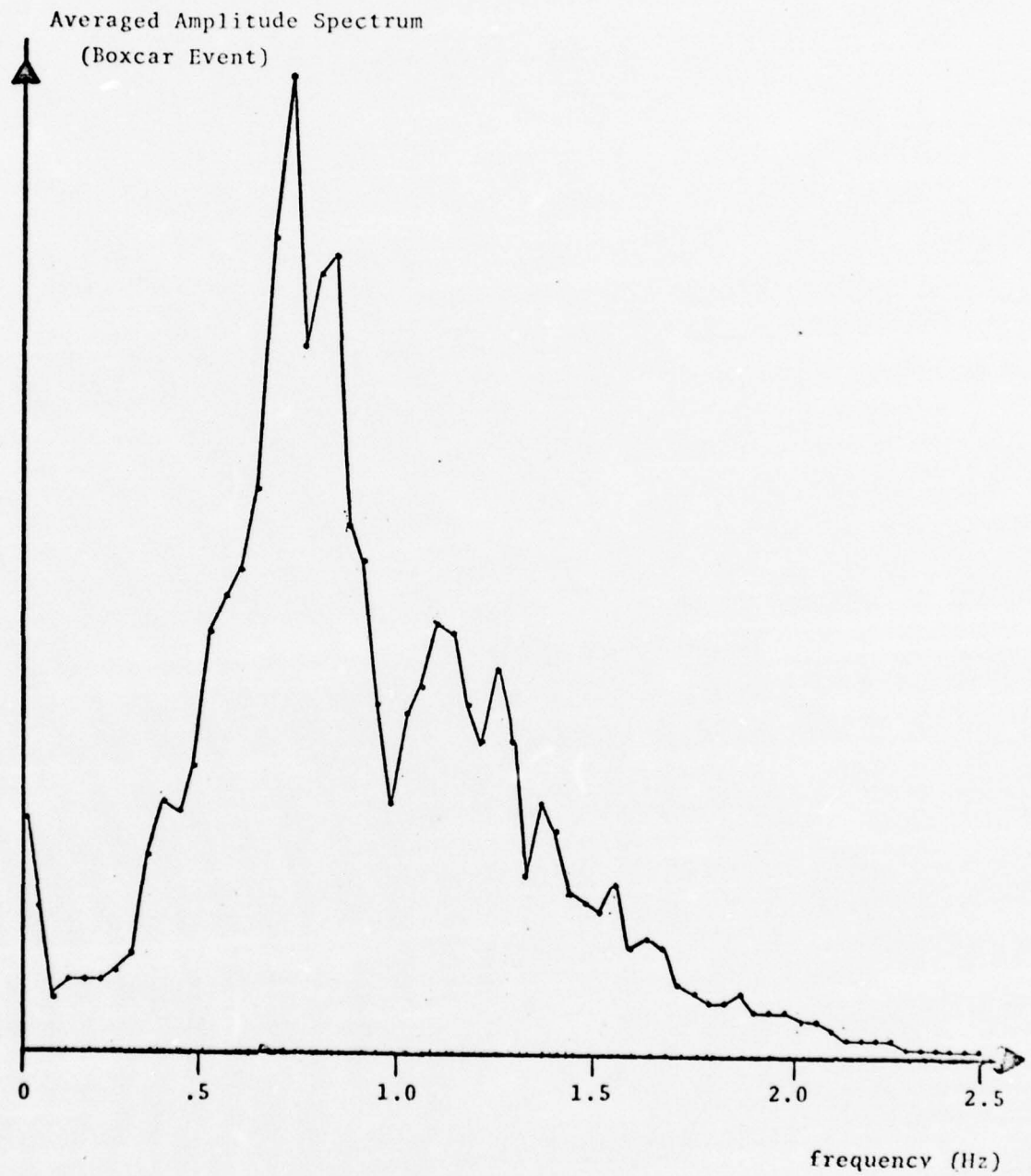


Figure 4.1.1b

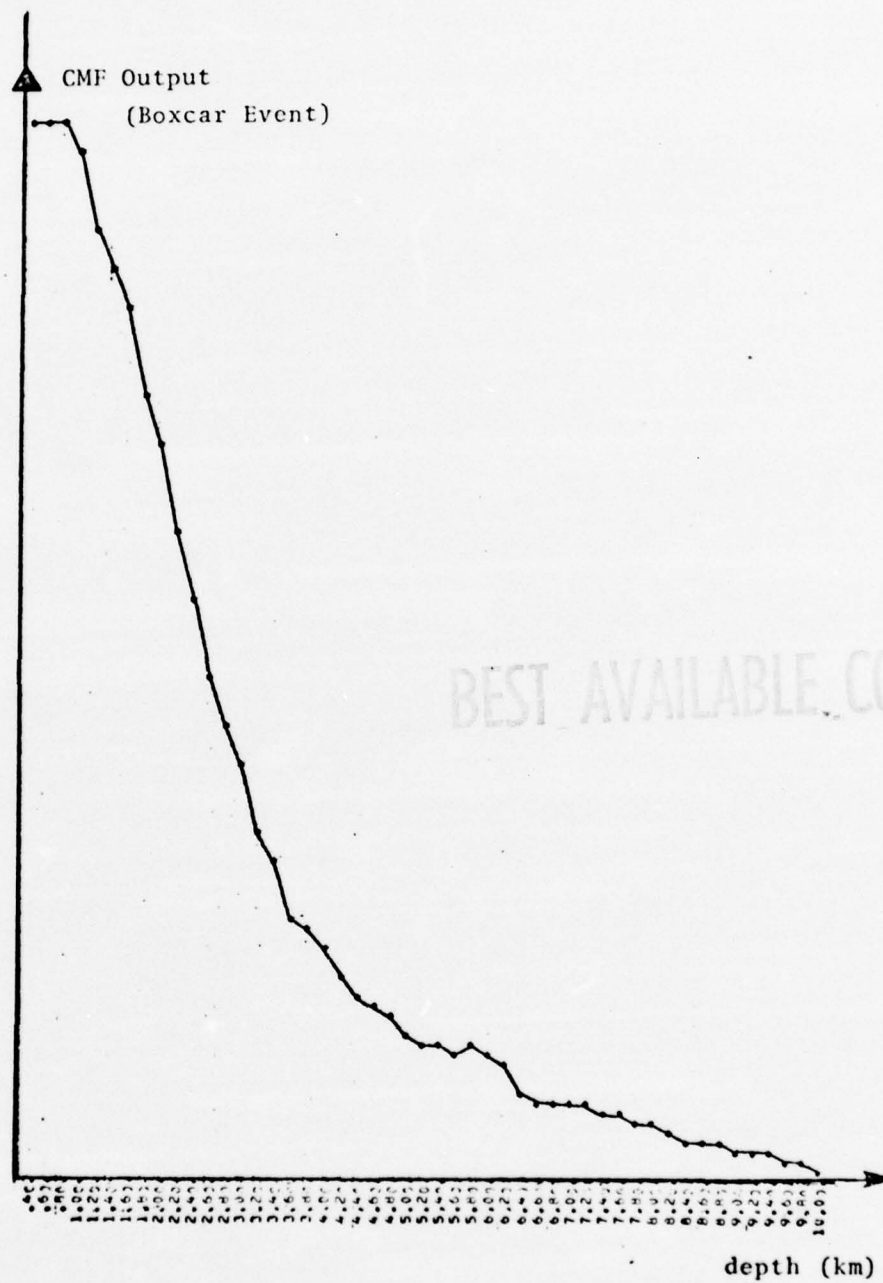


Figure 4.1.2

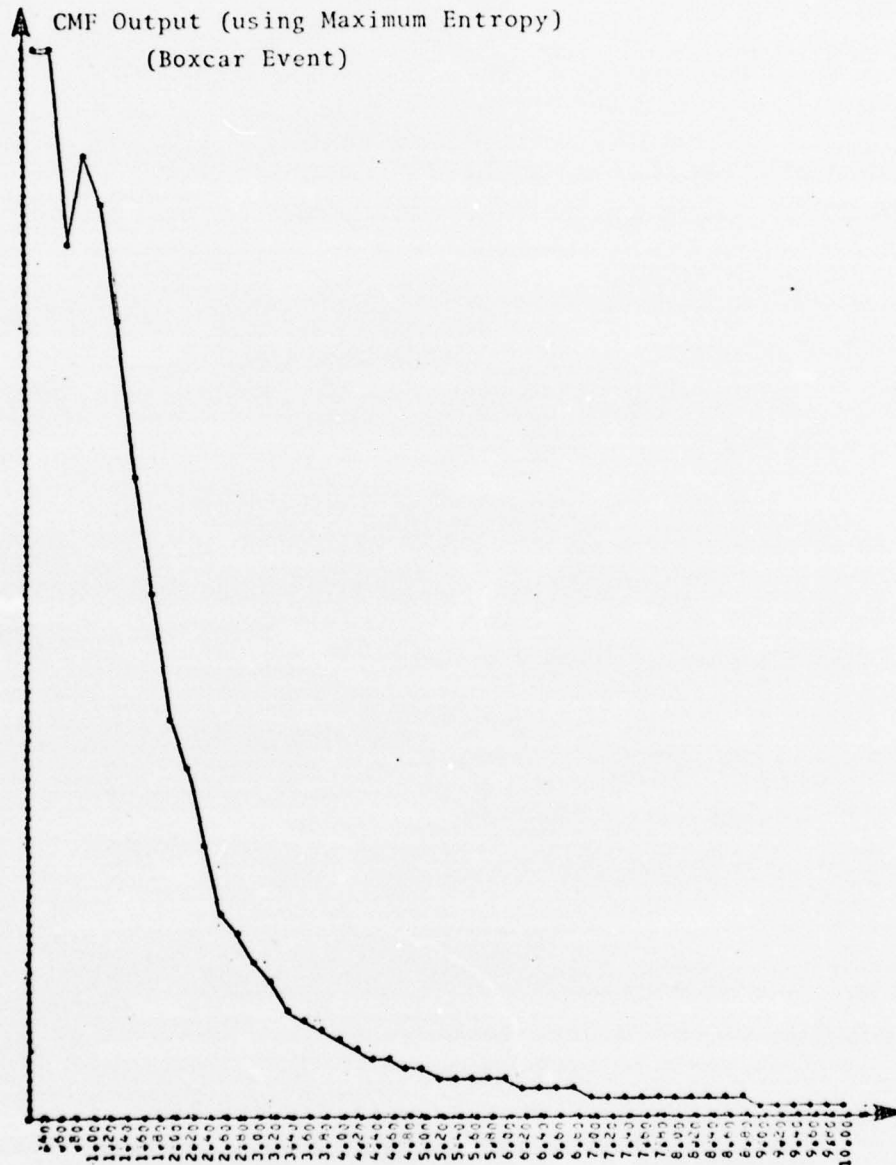


Figure 4.1.3

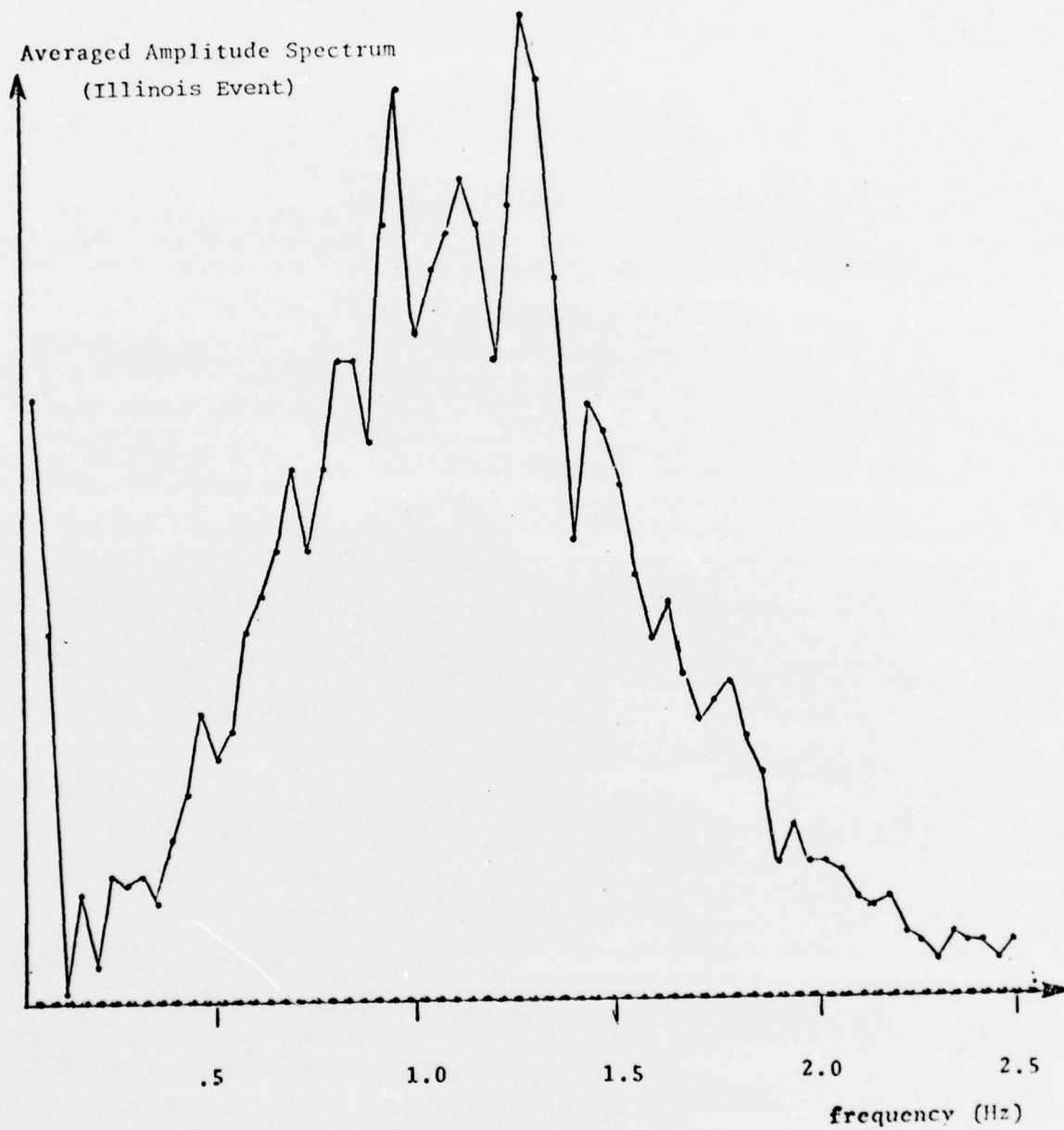


Figure 4.1.4

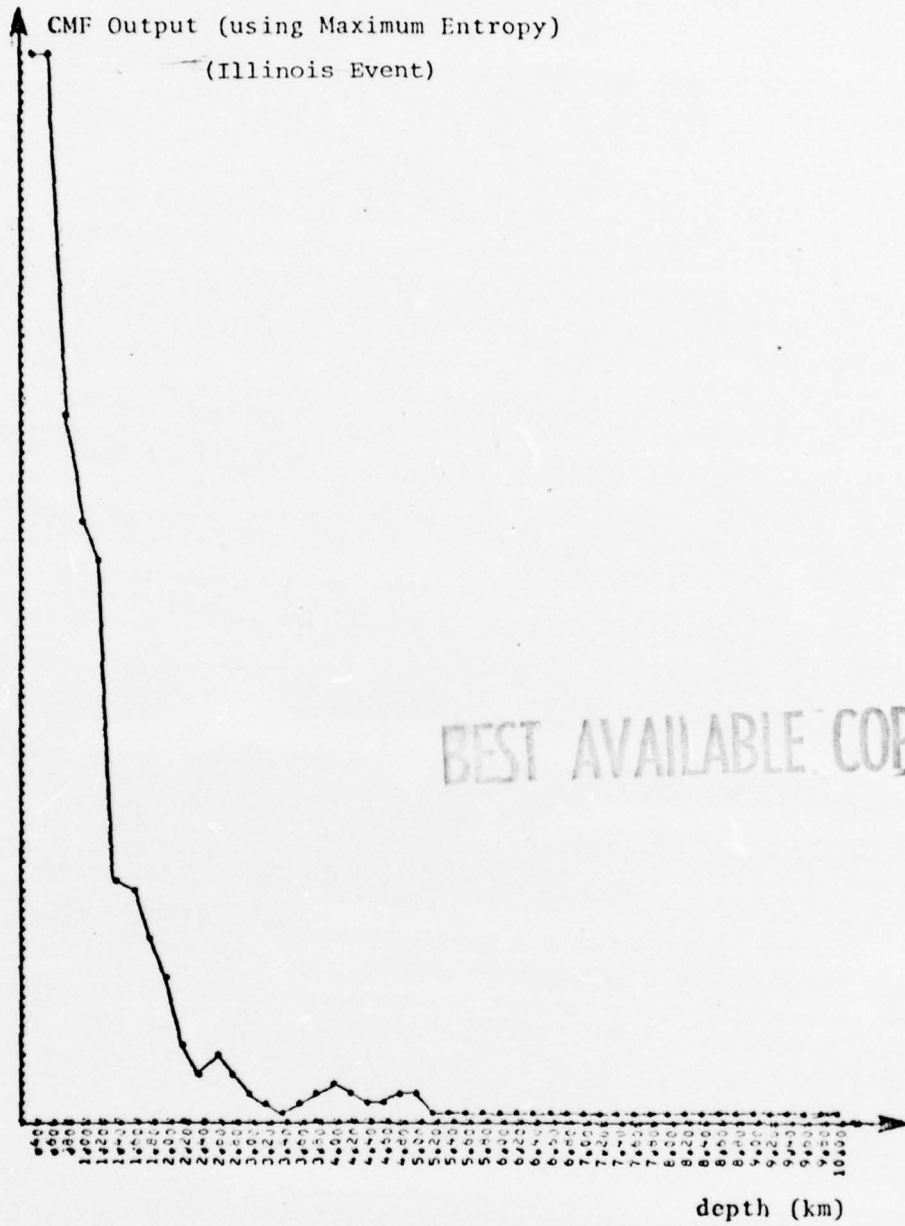


Figure 4.1.5

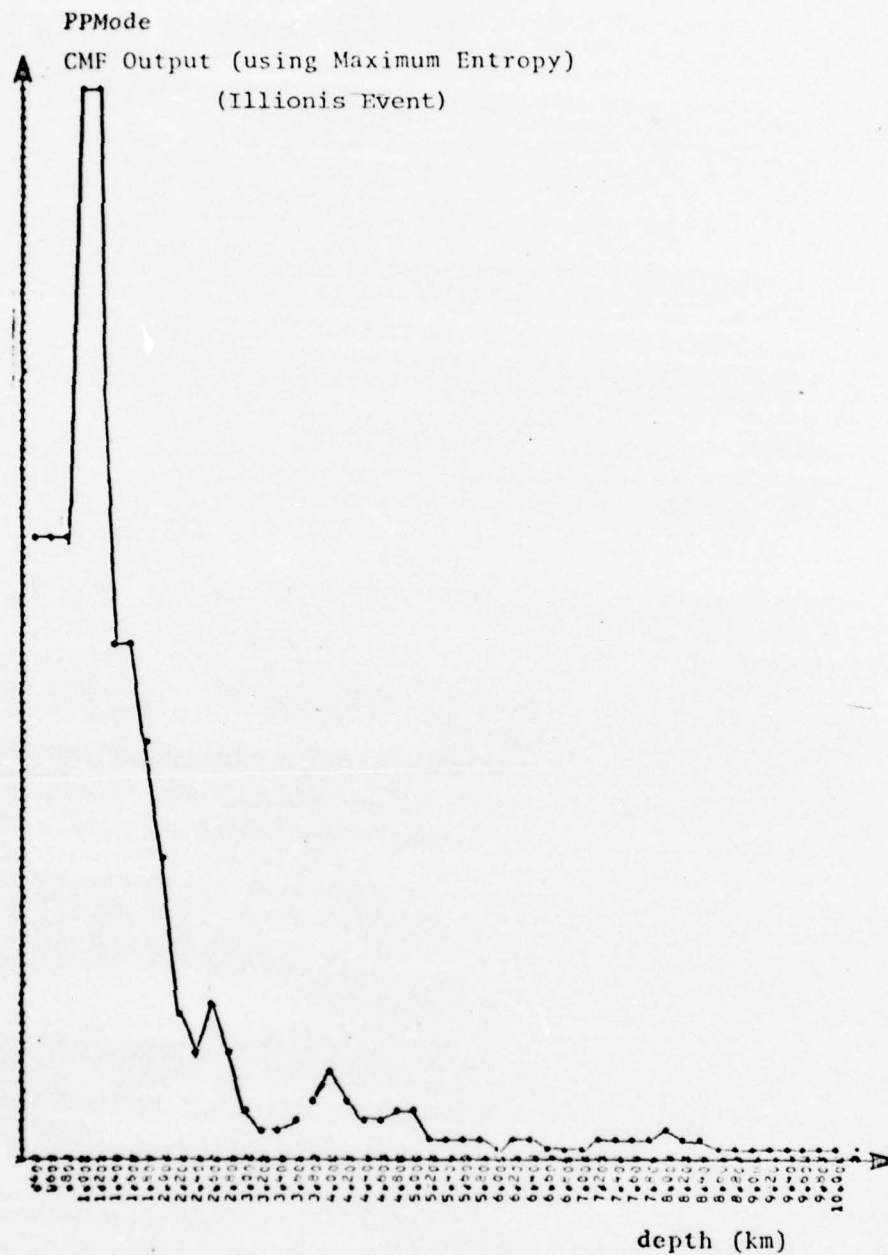


Figure 4.1.6

Figures 4.1.7 and 4.1.8 show the results of the analysis for the Boxcar and Illinois Events (not using Maximum Entropy) with the depth analysis carried out to 60 km and the mean of the amplitude spectrum removed. One notes the greater structure at depths >10 km from the Illinois Event compared with these from the Boxcar Event. One sees peaks at 25 km and 37 km corresponding to the pP-P and sP-P time delays for the Illinois Event. (The sP-P delay shows up since the CMF was not used in the run and this energy was not folded back into the pP-P peak.) This additional structure may prove to be a discriminate for natural event.

4.2 Determination of the Effectiveness of Cepstrum Analysis for Shallow Source Depths Using Synthesized Data

In order to determine the effectiveness of the cepstrum technique in determining depths for shallow events, seismograms were synthesized to simulate events having surface reflected delay times of 1.5, .75, .4 and .25 seconds corresponding to depths of 5, 2.5, 1.3 and .83 km for epicenter distances of $\sim 40^\circ$. This was accomplished by delaying and summing Boxcar seismograms to themselves (to insure realistic signal bandwidths in the synthesized seismogram) at delays corresponding to given source depths.

For each of the time delays used, seismograms were generated for five stations each having seven coda pieces of 256 sample points. The automated source depth analysis procedure was used to compute an average weighted cepstrum from this data. A differential cepstrum was also computed by scaling and subtracting from these cepstrums the cepstrums computed from the seismograms not containing the simulated surface reflection. The

BEST AVAILABLE COPY

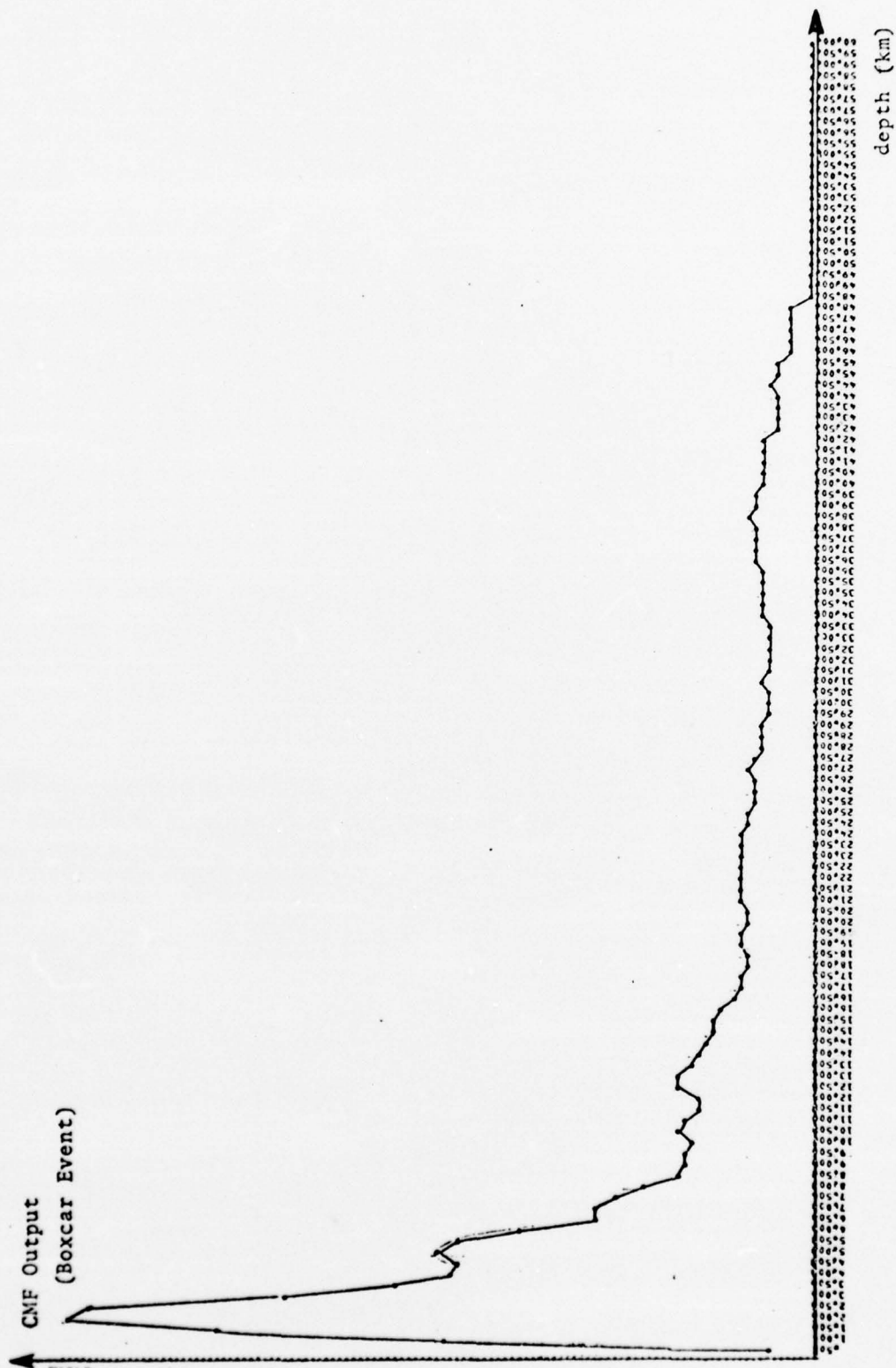


Figure 4.1.7

BEST AVAILABLE COPY

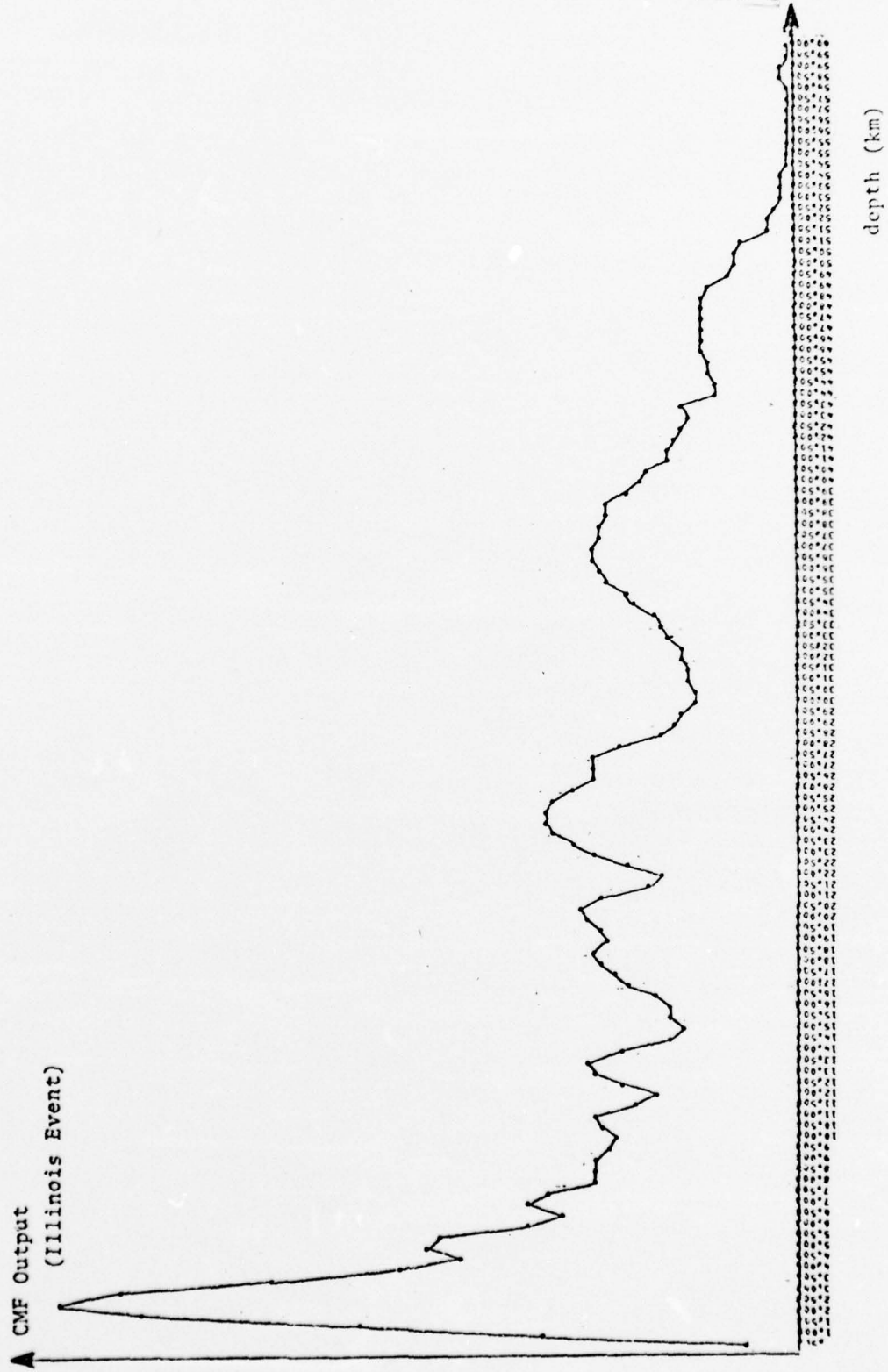


Figure 4.1.8

subtraction technique has the advantage of removing those cepstrum features which are generated from the source waveform alone. Although it is not obvious that this technique can be used with real data it is useful in determining the limitations of the cepstrum technique for these situations. However, with additional information such as surface shots and/or use of the theoretical relationships between waveforms generated at different depths and yields, such a procedure could be effective.

Figures 4.2.1a and 4.2.1b show the resulting averaged cepstrum and averaged differential cepstrum for a time delay of 1.5 seconds. The peak at 1.5 seconds is seen in both cepstrums but is much more evident in the differential cepstrum as can be expected since the common cepstrum features have been removed, leaving only the feature due to the simulated surface reflection. Figures 4.2.2a and 4.2.2b show similar plots for a time delay of .75 seconds. Here the advantage of the differential cepstrum becomes obvious in giving a clear peak at .75 seconds versus only an inflection in the cepstrum computation. Figures 4.2.3a and 4.2.3b show a case in which the time lag has been reduced to .4 seconds, where there is no indication of the time lag in the averaged cepstrum but is again very clear in the differential cepstrum. Finally, we used a delay of .25 seconds and plots of Figures 4.2.4a and 4.2.4b indicate that the differential cepstrum is still capable of detecting this time lag but the signal/noise ratio has greatly deteriorated; primarily a consequence of the short delay and bandlimited signal. The analyses of these synthesized seismograms were performed to indicate what one can expect from cepstral analysis for shallow depth phase detection for realistic signal bandwidths. A result of this research is that one needs to develop techniques which allow the estimation of cepstrum features originating from the source waveform not containing the surface reflection in order to detect delay times of <1 second.

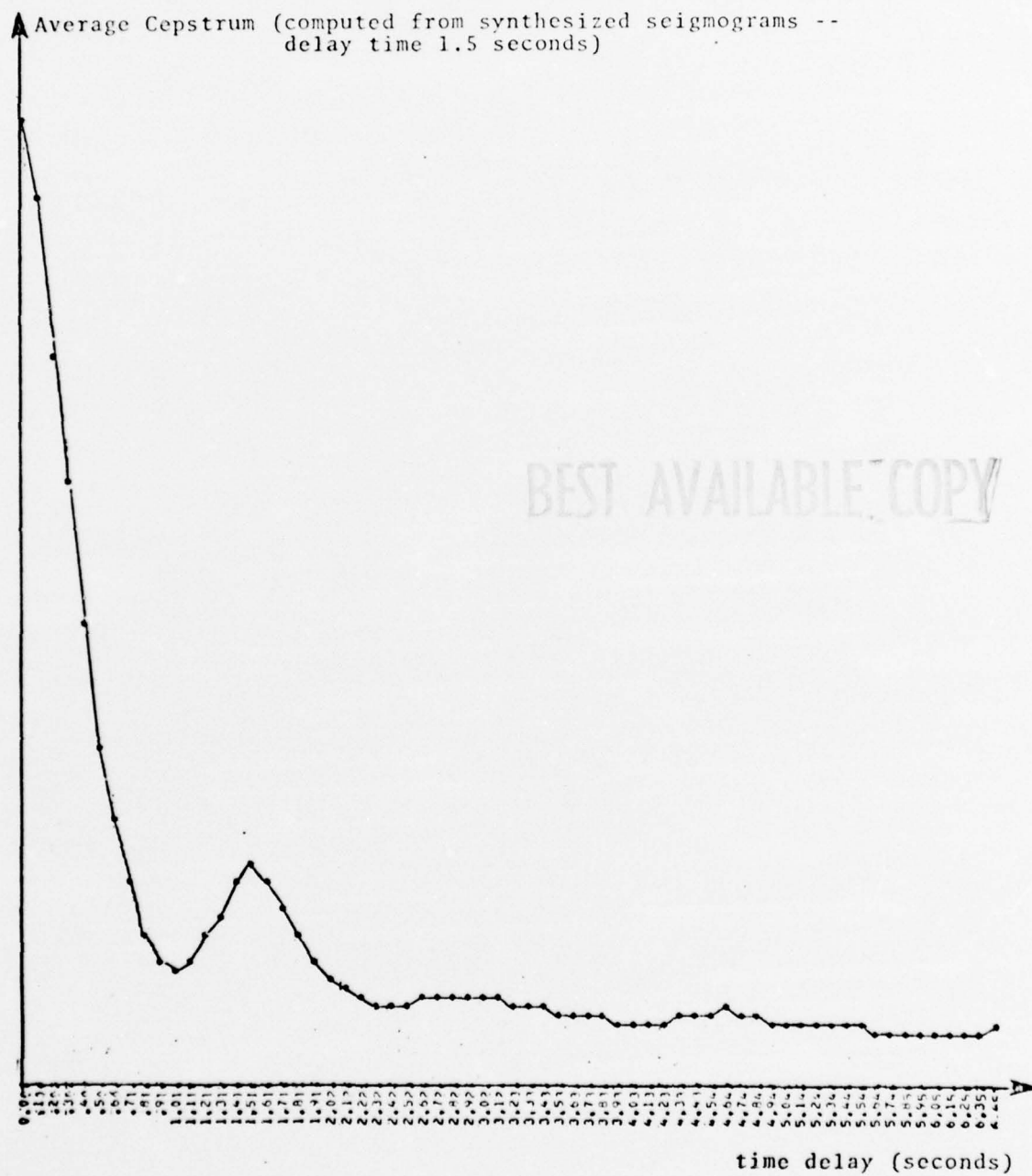


Figure 4.2.1a

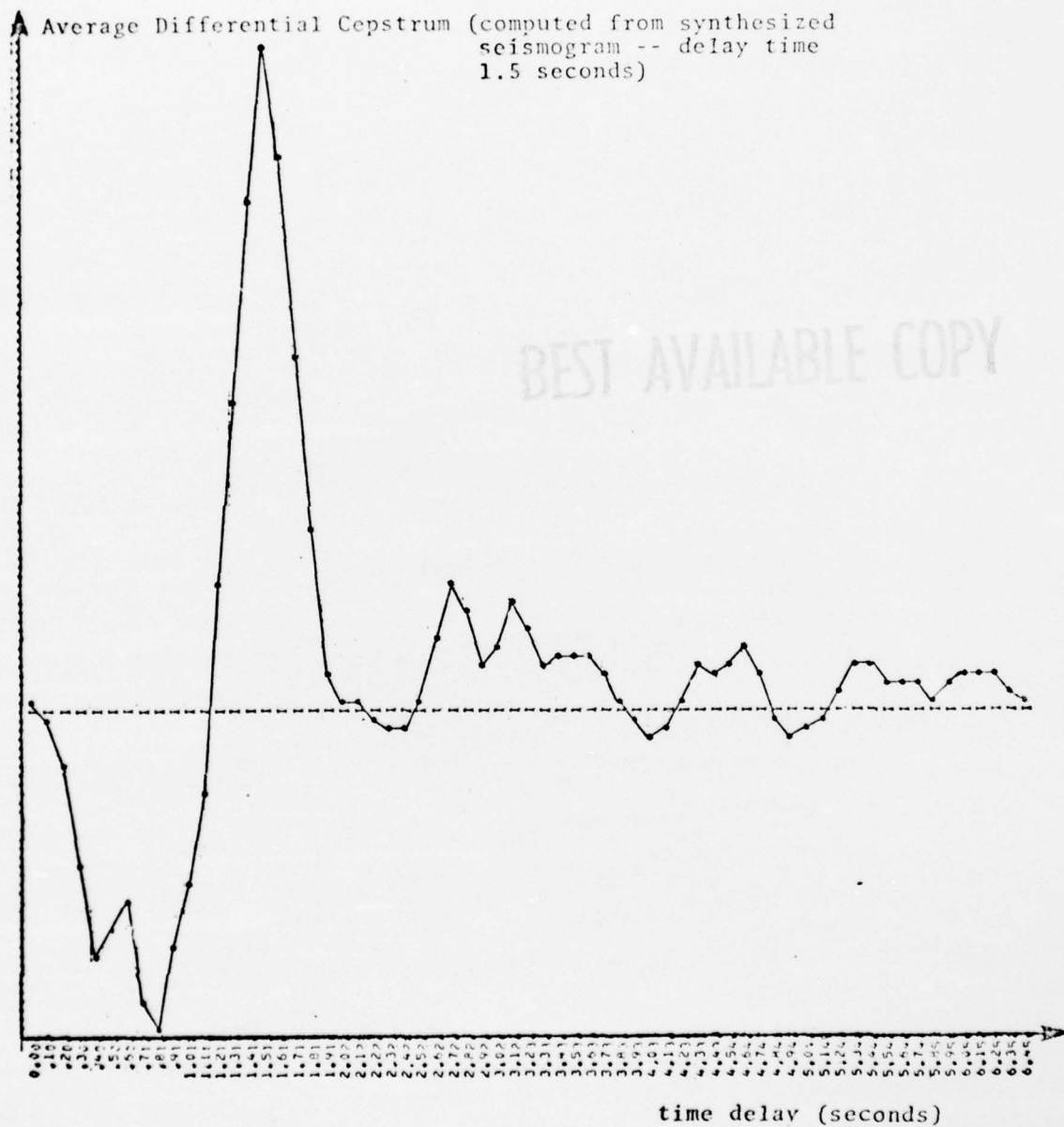


Figure 4.2.1b

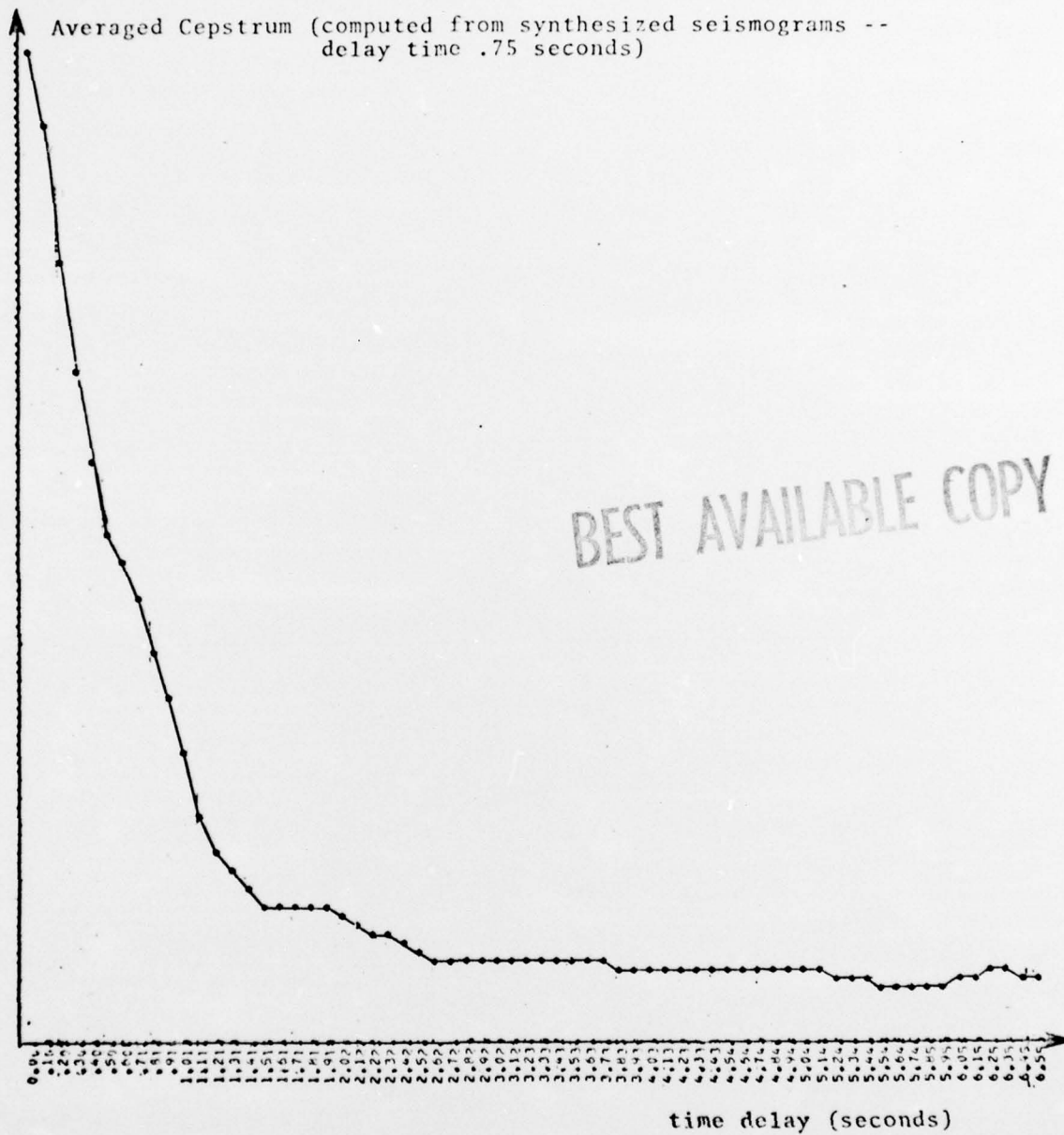


Figure 4.2.2a

BEST AVAILABLE COPY

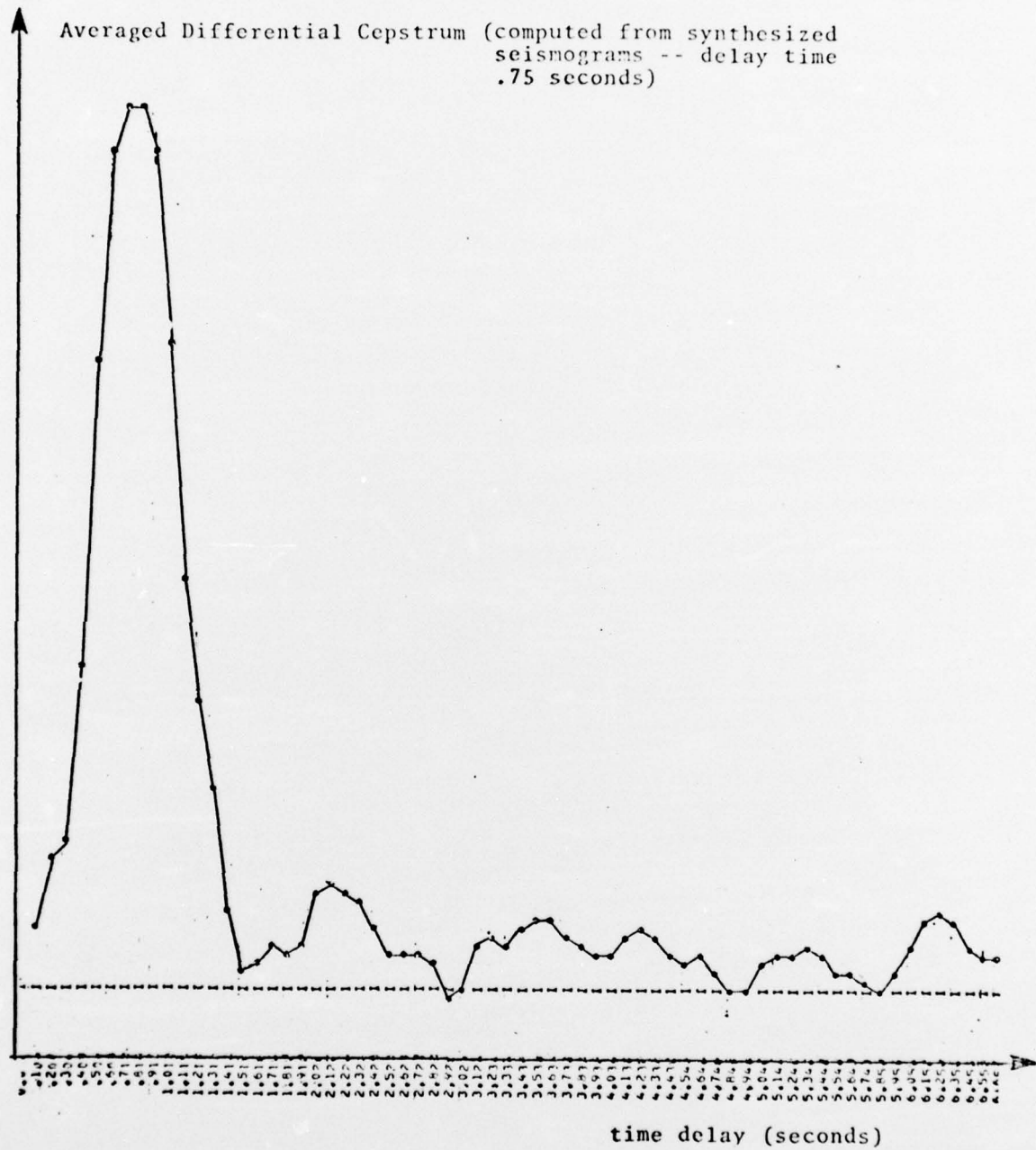


Figure 4.2.2b

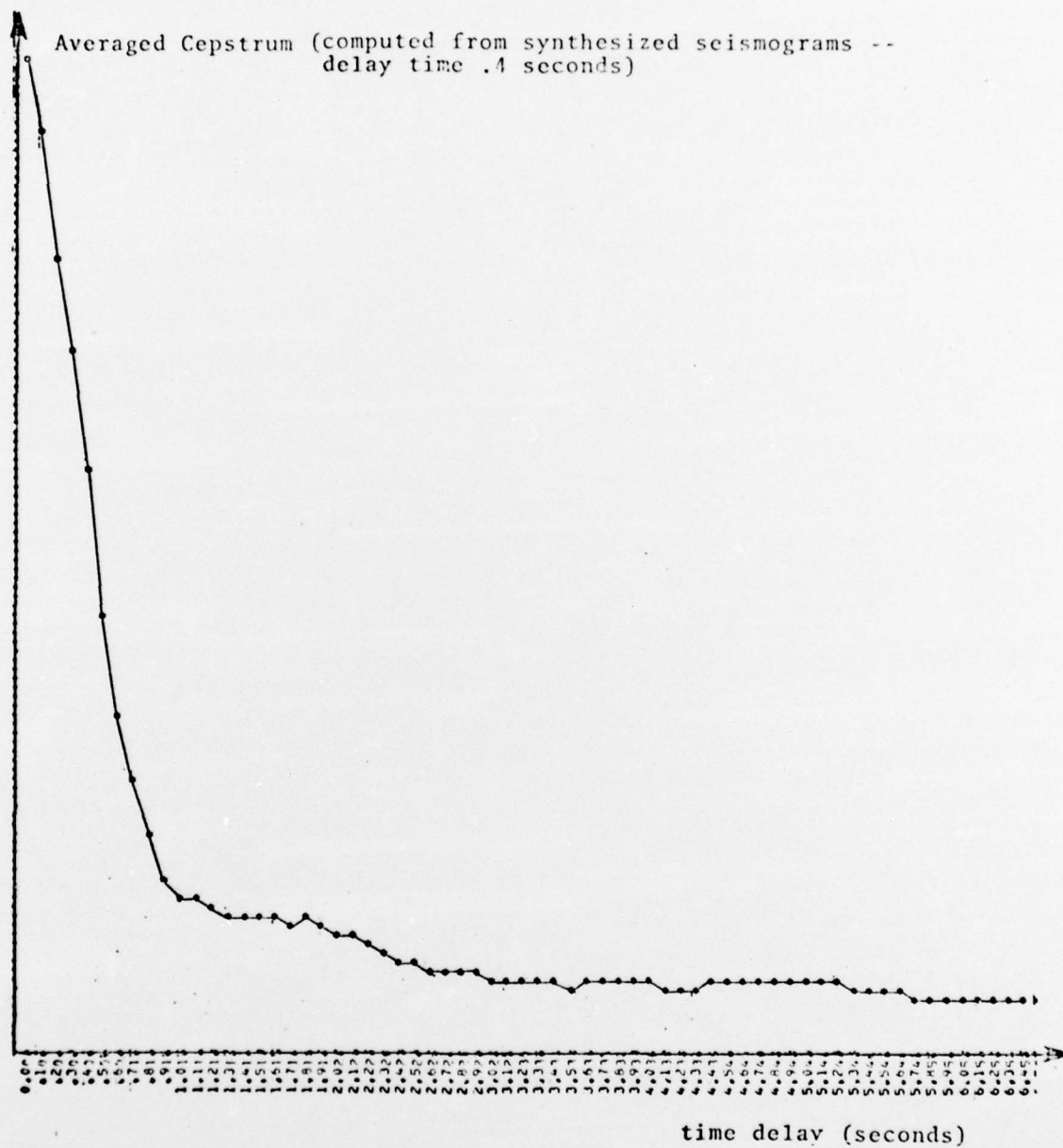


Figure 4.2.3a

BEST AVAILABLE COPY

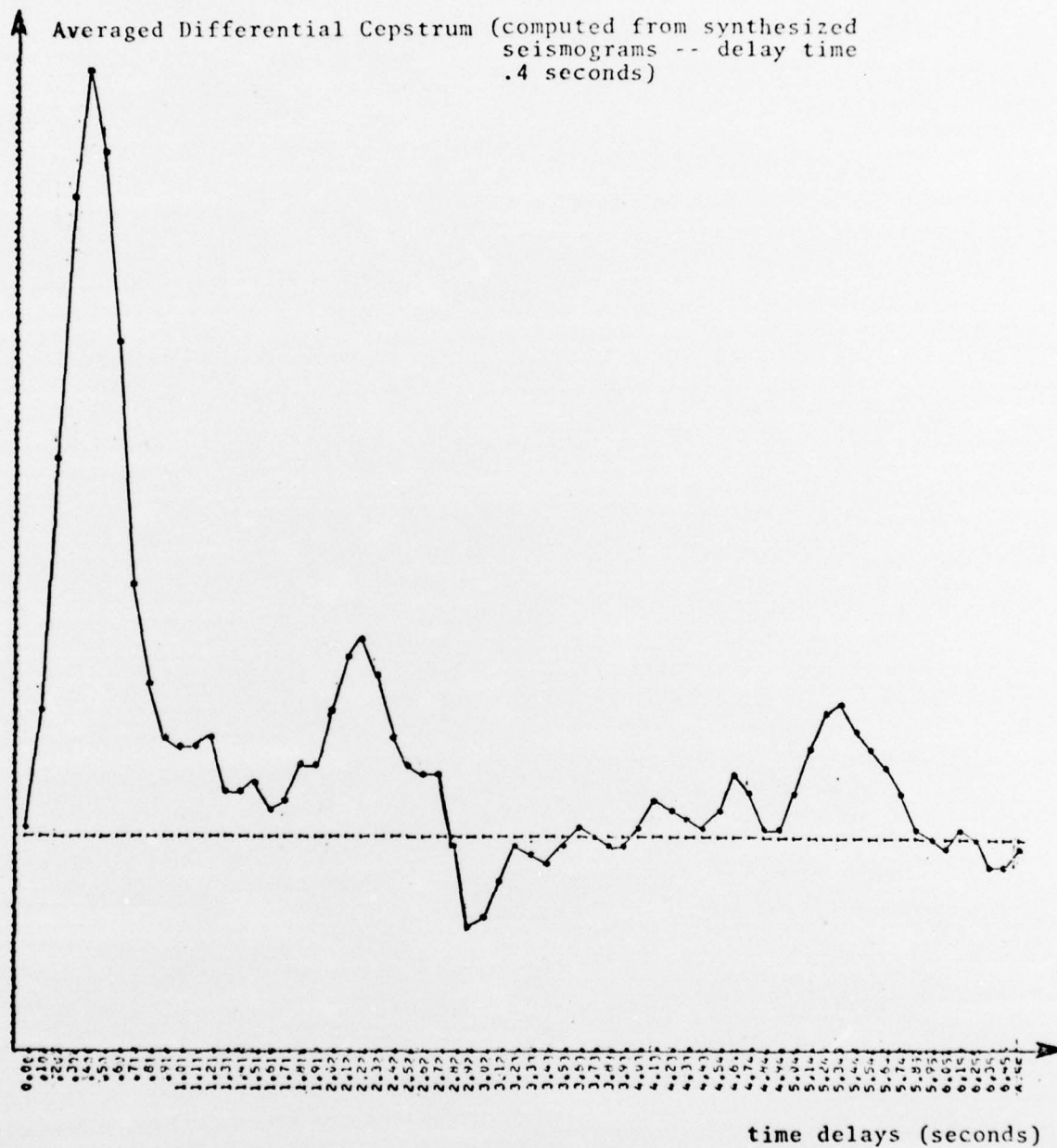


Figure 4.2.3b

BEST AVAILABLE COPY

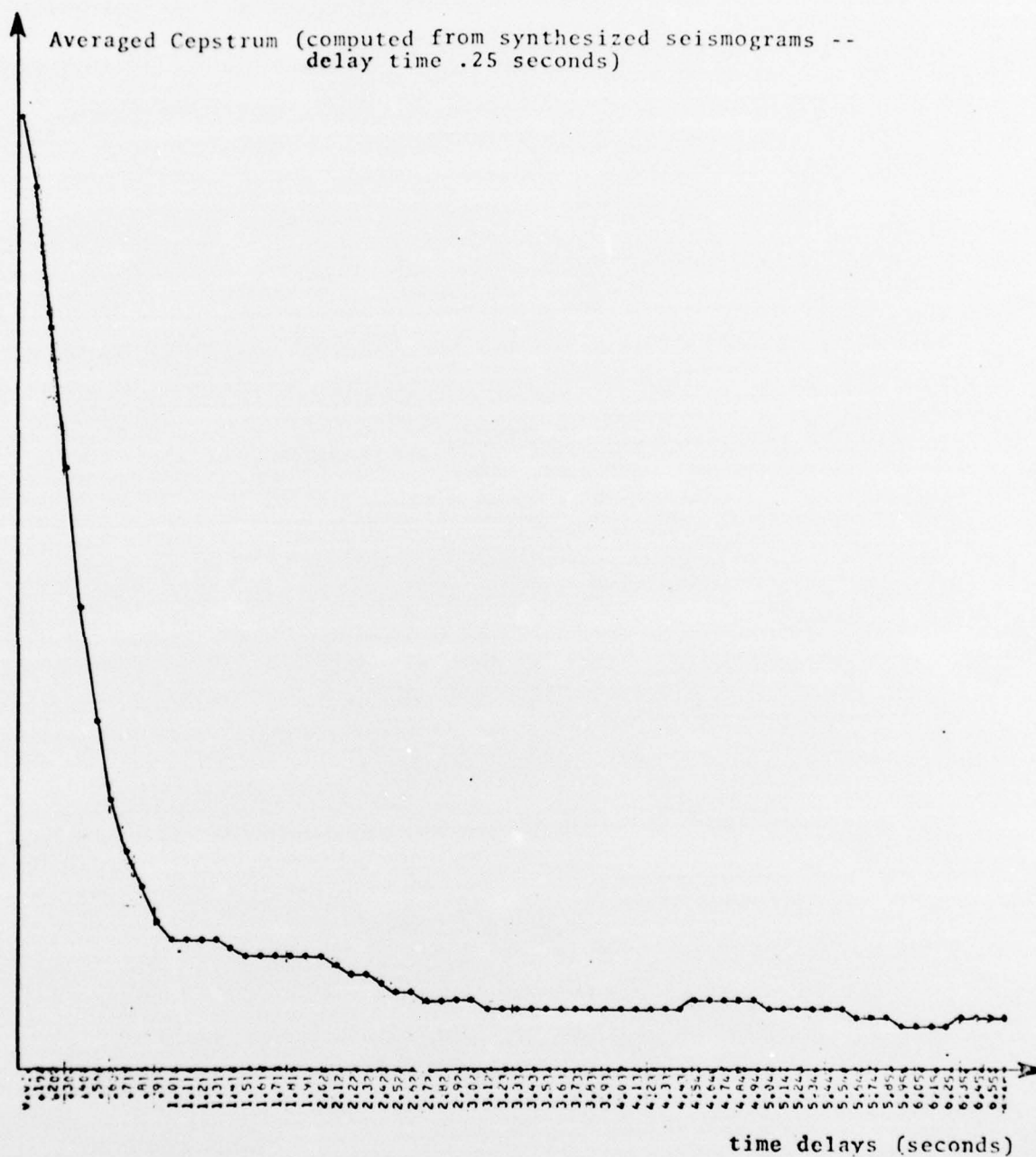


Figure 4.2.4a

BEST AVAILABLE COPY

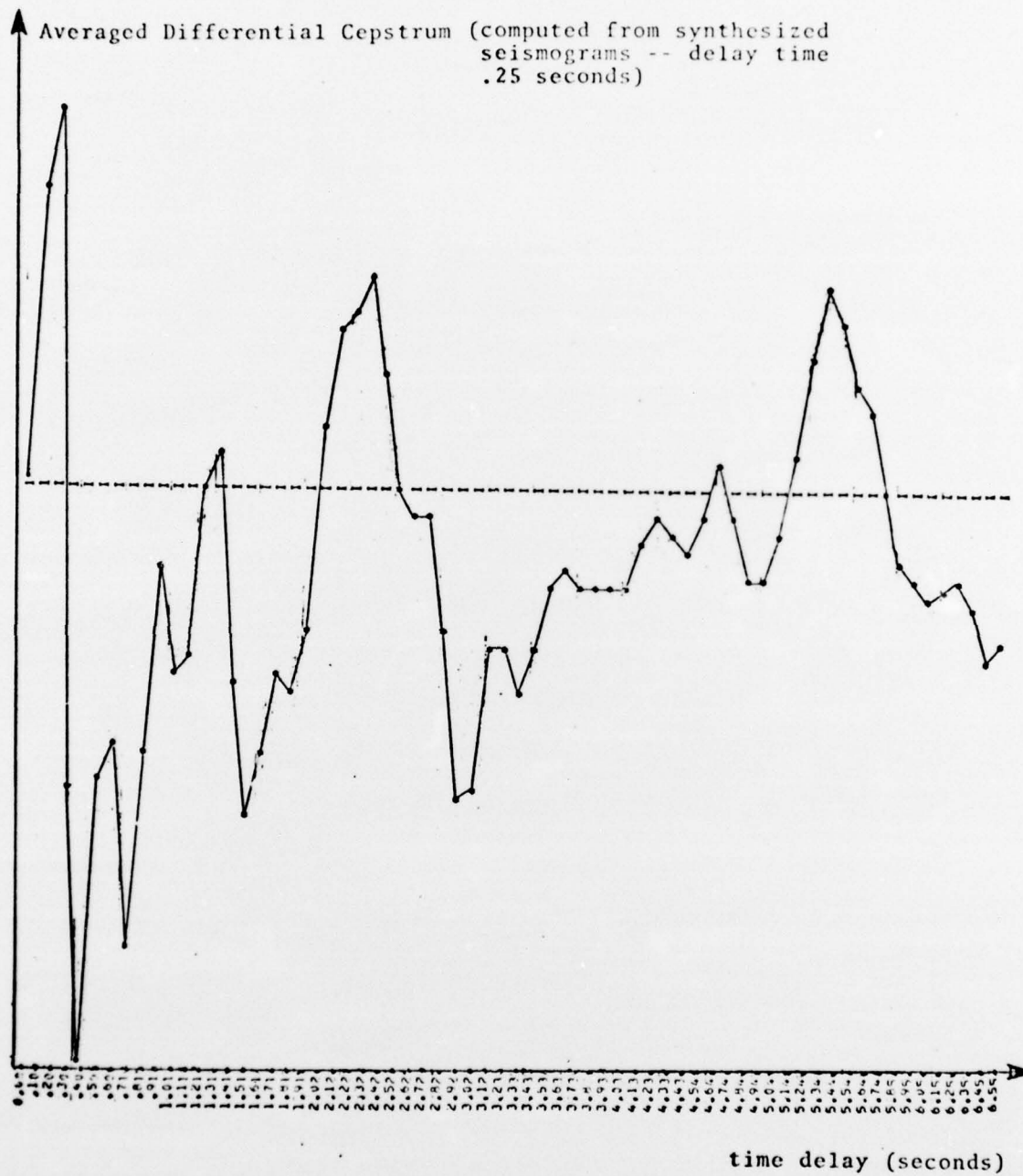


Figure 4.2.4b

5.0 CONCLUSION

During this contract, an automated teleseismic source depth determination analysis has been developed for events having source depths in the 50-200 km range, and was applied to seismic event data. It was demonstrated that through this analysis, source depth information contained throughout the seismogram is being constructively utilized to obtain source depth estimates. It was also demonstrated that this analysis gives correct source depths from data recorded at individual stations for the Illinois Event. These capabilities should allow one to obtain source depths for a considerably higher percentage of seismic events.

Research was conducted to establish possible modifications to the analysis which would enhance its effectiveness for events having source depths less than 5 km. A result of this research was that in order to use the cepstrum analysis approach for shallow events, techniques to determine cepstrum features resulting from the direct seismic arrival (those not containing the surface reflected arrival) need to be developed.

To establish the general applicability and conditional limitations of the source depth analysis, a large set of events must be analyzed. In addition, techniques to establish the significance and estimated error in these depth determinations should be included in the analysis procedure.

APPENDIX A
COMPUTATION OF CEPSTRUM

The following steps are used to calculate the Stochastic Cepstrum for a seismogram consisting of NS consecutive portions each having N amplitude values:

- Select N sampled (sample rate = 20 pts/sec) amplitude values from the Mth portion of a seismogram

$$X_M(n), n=0, 1, \dots, N-1$$

and add N zeroes to interpolate the spectrum

- Calculate the amplitude spectrum for positive frequencies using

$$A_M(j) = \left| \frac{1}{2N} \sum_{n=0}^{2N-1} X_M(n) e^{-2\pi i n j / 2N} \right| ; j=0,1,\dots, N-1$$

with the Nyquist frequency = 10 Hz and $i = (-1)^{1/2}$.

- Retain only the lower quarter frequencies of the amplitude spectrum since there is very little energy at frequencies above 2.5 Hz for natural events. This leaves the array

$$(A_M(j), j = 0, 1, \dots, N/4-1)$$

- Remove the mean and apply a cosinusoidal taper to the first 10% and last 20% of the A_M array giving the modified array

$$(A'_M(j), j = 0, 1, \dots, N/4-1)$$

The 20% taper on the higher frequencies was used to de-emphasize the higher frequencies

- Add $N/4$ zeroes to interpolate the cepstrum giving the array

$$(A'_M(j), j = 0, 1, \dots, N/2-1)$$

At this stage one would take the log of this A'_M array to obtain the log cepstrum; but by not using the log better results were obtained.

- Calculate the Fourier Transform of the A'_M array using

$$F_M(k) = \frac{1}{N/2} \sum_{j=0}^{N/2-1} A'_M(j) e^{-2\pi i j k / (N/2)}$$

where $(F_M(k), k = 0, 1, \dots, N/4-1)$ are

complex numbers representing the positive frequency spectrum of A_M . One can now obtain the amplitude and phase of each cepstrum point k . The array

$(|F_M(k)|, k = 0, 1, \dots, N/4-1)$ is what we

is referred to as the cepstrum amplitude and the complex numbers $F_M(k)$ are referred to as cepstrum phasors.

- To calculate the stochastic cepstrum, one then calculates

$$|F_M(k)| = \text{Max} (|F_M(j)|, j = k-\Delta/2, k+\Delta/2)$$

for each section M and sums these over the number of sections (NS) used from a given seismogram (Δ is the stochastic window width). This gives

$$C(k) = \sum_{M=1}^{NS} |F_M(k)| \cdot w_M ,$$

where $C(k)$ is the stochastic cepstrum and w_M is a weighting factor, chosen such that the mean amplitude of each $|F_M(k)|$ array is equal.

APPENDIX B

CEPSTRUM MATCHED FILTER (CMF)

If one assumes that the cepstral peaks appearing at the pP-P, sP-P and sP-pP time delays dominate the expected cepstrum pattern for an event, then one can formulate the CMF algorithm in the following way. Consider the cepstrum to consist of N amplitude values $CP(n)$ for the time delays $t_n = (n-1) \cdot \Delta t$, where $n = 1, 2, 3, \dots, N$. Then the synthetic cepstrum (CS) expected for an event at a given depth and distance corresponding to a pP-P delay time of τ , can be represented by:

$$CS(n, \tau, \alpha) = Q(n, (\alpha-1)\tau) + Q(n, \tau) + Q(n, \alpha\tau)$$

with $\alpha = T_{sP-P}/T_{pP-P}$, and is the ratio of delay times for sP-P and pP-P. Also Q is defined by

$$Q(n, \tau) = 1 ; \text{ if } \tau - \Delta t < t_n < \tau + \Delta t , \\ = 0 ; \text{ otherwise .}$$

Thus, CS is represented by three unit amplitude peaks located at the sP-pP, pP-P, and sP-P delay times, each peak consisting of three adjacent delay time points.

The CMF output at time delay τ is defined to be the maximum zero lag correlation of the computed cepstrum (CP) with the synthesized cepstrum (CS) for a source depth having a pP-P delay time τ computed over a range of ratios α . This can be written as

$$\begin{aligned}
\text{CMF}(\tau) &= \text{Max}_{\alpha_1 \leq \alpha \leq \alpha_2} \left\{ \sum_{n=1}^N \text{CP}(n) \cdot \text{CS}(n, \tau, \alpha) \right\} ; \begin{array}{l} \text{if } \text{CP}(\tau) > .7 \cdot \text{CP}(\alpha\tau) \\ \text{and } \text{CP}(\tau) > .7 \cdot \text{CP}((\alpha-1)\tau) \end{array} \\
&= \text{CP}(\tau) ; \text{otherwise}
\end{aligned}$$

Here, α_1 and α_2 are set from the expected range of values for α for a given range of possible depths. Values of $\alpha_1 = 1.25$ and $\alpha_2 = 1.55$ were used for the event distances and depths encountered in this research. The constraints imposed require that the amplitude of the cepstrum peak at τ must be at least .7 times the amplitude of the cepstrum peaks at both $\alpha\tau$ and $(\alpha-1)\tau$. This eliminates detection of cepstral patterns for cases in which the strength of the pP arrival is considerably less than that of the sP arrival. Thus, a cepstrum peak at τ resulting from a pP arrival for an event will not contribute to the CMF output for an apparent event having an expected sP-P delay time of τ , without the significant presence of a pP arrival for this apparent event.

As an example of the application of this technique, consider Figure 1. At the top of the figure is the cepstrum calculated from an event of known depth having both the pP and sP depth phases clearly identifiable. This cepstrum pattern is dominated by three peaks corresponding to the sP-pP, pP-P, and sP-P delay times. Upon interpreting this cepstrum for an unknown event depth, one sees that each of the three peaks has the possibility of corresponding to the pP phase. The CMF output is plotted at the bottom of Figure 1 and indicates a much stronger emphasis on the peak corresponding to the correct pP-P delay time for this event. This result reflects the fact that this cepstrum pattern, primarily

consisting of three peaks, is in strong agreement with the pattern expected for a single event having this pP-P delay time. The lesser probability that the relative location of these three peaks was coincidental, and that one of the other two peaks actually corresponded to the correct pP-P delay time, is indicated by the presence of CMF output peaks at those delay times having reduced amplitudes.

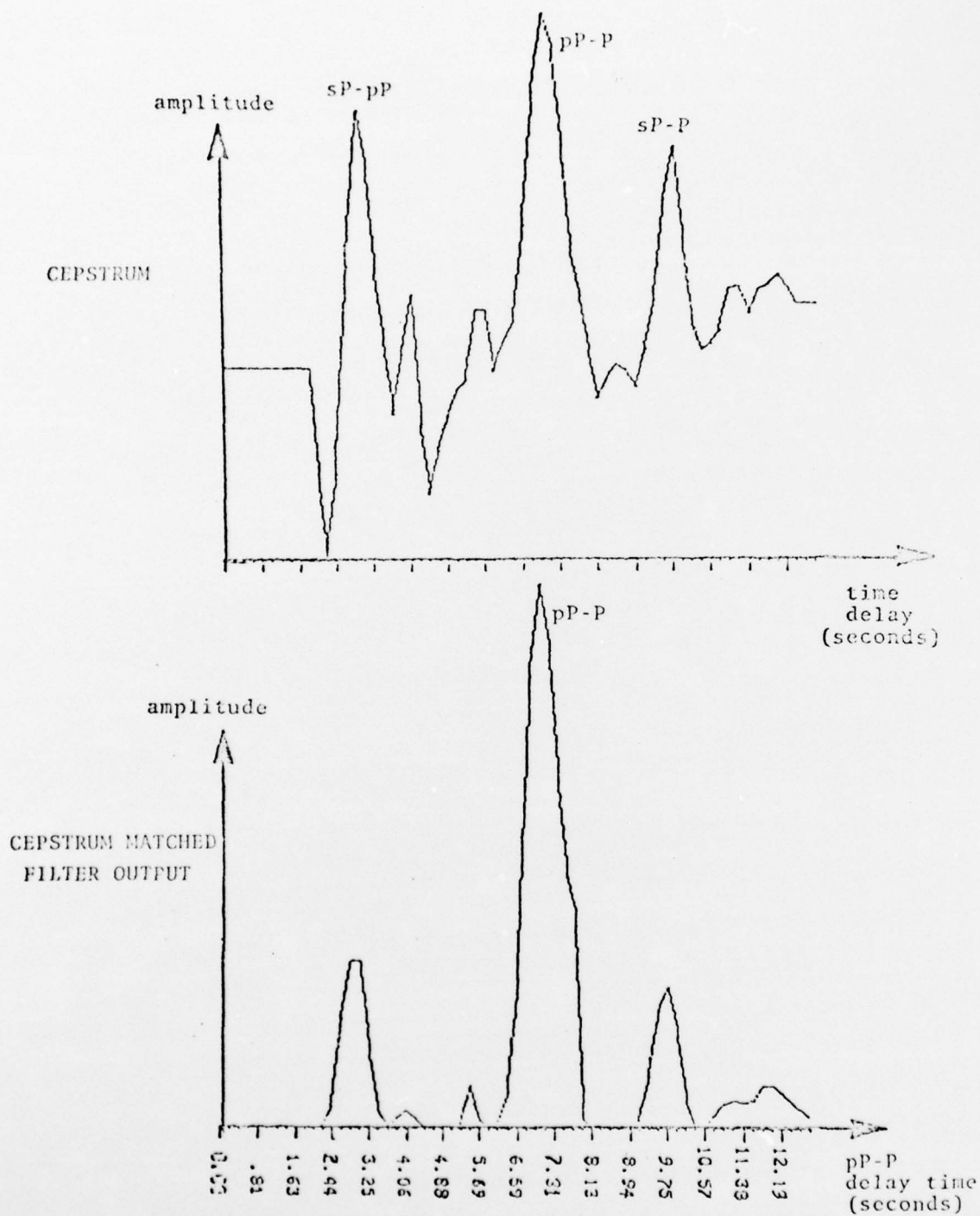


Figure 1. Cepstrum and Cepstrum Matched Filter output computed from data recorded at several stations for an event with well defined depth phases.